Quaternary glaciation of Muztag Ata and Kongur Shan: Evidence for glacier response to rapid climate changes throughout the Late Glacial and Holocene in westernmost Tibet

Yeong Bae Seong†
Lewis A. Owen
Department of Geology, University of Cincinnati, Cincinnati, Ohio 45221, USA

Chaolu Yi
Institute of Tibetan Plateau Research, Chinese Academy of Sciences, Beijing, 100085, China

Robert C. Finkel
Center for Accelerator Mass Spectrometry, Lawrence Livermore National Laboratory, Livermore, California 94550, USA

ABSTRACT

The glacial geology of two massifs, Muztag Ata and Kongur Shan, in western Tibet was examined to help define the timing and style of glaciation in the semiarid regions of western Tibet. Remote sensing, geomorphic mapping, and ^{10}Be terrestrial cosmogenic nuclide (TCN) surface-exposure dating of boulders on the moraines and sediment in depth profiles show that glaciers advanced at least 12 times during at least the last two glacial cycles. Over this time, the style of glaciation changed progressively from one that produced ice caps to one that produced less extensive and more deeply entrenched valley glaciers. The timing of the two earliest glaciations is poorly defined, but they likely occurred prior to the penultimate glacial cycle (the Karasu glacial stage) and the early part of the last glacial cycle or during the penultimate glacial cycle (the Subaxh glacial stage). In contrast, the timing of later glacial advances (the Olimde glacial stage) is relatively well defined showing quasiperiodical oscillations on millennial time scales (17.1 ± 0.3 ka, 13.7 ± 0.5 ka, 11.2 ± 0.1 ka, 10.2 ± 0.3 ka, 8.4 ± 0.4 ka, 6.7 ± 0.2 ka, 4.2 ± 0.3 ka, 3.3 ± 0.6 ka, 1.4 ± 0.1 ka, and a few hundred years before the present). These data suggest that since the global Last Glacial Maximum (LGM), the glaciers in western Tibet likely responded to Northern Hemisphere climate oscillations (rapid climate changes), with minor influences from the south Asian monsoon. This study provides the first well-defined glacial geologic evidence to suggest that glaciers in western Tibet respond to rapid climate changes on millennial time scales throughout the Late Glacial and Holocene.

Keywords: glacial geology, Tibet, Muztag Ata, Kongur Shan, geochronology, terrestrial cosmogenic nuclide surface-exposure dating, midlatitude westerlies, Late Glacial, Holocene, rapid climate changes.

INTRODUCTION

The Tibetan Plateau and its neighboring mountains have a profound connection to global and regional climate (Ruddiman and Kutzbach, 1989; Molnar and England, 1990; Prell and Kutzbach, 1992; Owen and Benn, 2005). Understanding the nature and dynamics of past climate in the region is therefore important, in a basic sense, for modeling regional and global climate change and, in a practical sense, for helping to assess the effect of climate change, mostly through hydrological impacts, on an area that is home to more than one third of the world's population. The economies of these populations, being agriculturally based, are especially sensitive to variations in climate and to the associated glaciological and hydrological responses.

The well-preserved moraine successions and valley fills that are present throughout Tibet and the bordering mountains reflect, to first order, the extent and timing of mountain glaciation. Since the mountain glaciers that produced these landforms respond sensitively to fluctuations in local and regional climate, dating these landforms allows a reconstruction of Late Quaternary climate and provides a tool for investigating the relationship between local and global climate change. This approach has recently been used in numerous studies throughout eastern, northern, and southern Tibet and the Himalaya and the Transhimalaya, which together comprise the monsoon-influenced regions of Tibet and the Himalaya (Porter, 1970; Shroder et al., 1993; Sharma and Owen, 1996; Richards et al., 2000a, 2000b; Phillips et al., 2000; Owen et al., 2001, 2002a, 2002b, 2002c, 2003a, 2003b; Tsukamoto et al., 2002; Finkel et al., 2003). However, little research has been undertaken on the glacial geology of the high mountain deserts at the western end of the Himalayan-Tibetan orogen, which lies at the extreme edge of monsoon influence. Noticeable exceptions include Fort and Peulvast (1995), Ono et al. (1997), and Owen et al. (2002b, 2002c, 2006). Furthermore, these studies concentrate on the Pleistocene glacial history, and little is known about the extent and timing of Holocene glacier oscillations.

To examine the nature of glaciation in the semiarid regions at the western end of the Himalayan-Tibetan orogen and to develop the first, high-resolution, Late Glacial and Holocene glacial chronology, we studied two adjacent massifs, Muztag Ata and Kongur Shan (Fig. 1). These massifs were chosen because they are very accessible, within a 12-hour drive by road from the city of Kashgar, and because they contain one of the best preserved succession of moraines and glacially eroded landforms in Tibet. Furthermore, today, these massifs and the adjacent regions of western Tibet receive most of their precipitation from westerly air masses that bring moisture from the Mediterranean,

†Corresponding author: ybseong@hotmail.com

GSA Bulletin; March/April 2009; v. 121; no. 3/4; p. 348–365; doi: 10.1130/B26339.1; 6 figures; 2 tables; Data Repository item 2008230.

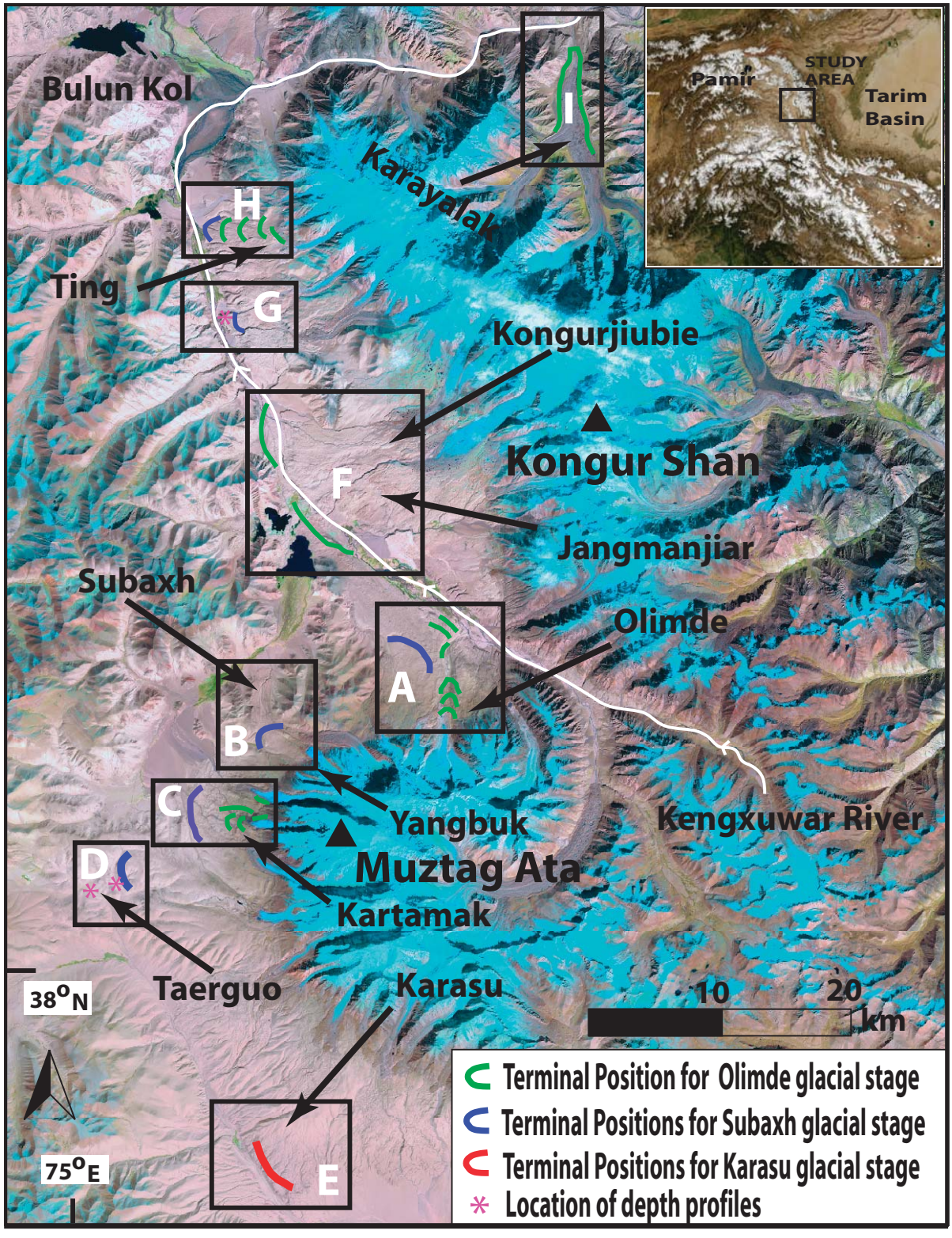

Figure 1. Landsat ETM+ (Enhanced Thematic Mapper Plus) image showing the glaciers on Muztag Ata and Kongur Shan. The moraines and terminal position of the main glacial advances for each of the detailed study areas examined in this project are highlighted in the black boxes and are shown in Figure 2. Please note that only the moraines that were dated are highlighted.

Black Sea, and Caspian Sea, with little, if any, monsoon influence (Aizen and Aizen, 1997; Barry and Chorley, 2003).

Remote sensing, field mapping, and sedimentological and geomorphic methods were applied to define the style and nature of glaciation in the region. Due to the lack of organic material suitable for ^{14}C dating, we applied ^{10}Be terrestrial cosmogenic nuclide (TCN) surface-exposure dating of boulders on the moraines and for sediment depth profiles. These data were used to test the hypothesis that Late Glacial and Holocene glaciation in semiarid western Tibet responds on millennial time scales to Northern Hemisphere climatic oscillations (rapid climatic changes of Denton and Karlen, 1973 and Mayewski et al., 2004). Furthermore, our study fills a large gap in the knowledge and understanding of the glaciation of the Himalayan-Tibetan orogen, which covers a vast geographical area, stretching ~2000 km × 1500 km.

STUDY AREA

Muztag Ata and Kongur Shan are situated at the westernmost end of the Tibetan Plateau and rise to 7546 and 7719 m above sea level (asl), respectively, from a plateau with an average elevation of ~3500 m asl. Both massifs are ~2000 m higher than any of the neighboring peaks and represent an area of significant anomalous topography (Schoenbohm et al., 2005; Seong et al., 2008; Fig. 1). Structurally they comprise anticlinal crustal domes, formed by the northward thrusting of the Kunlun terrane over the crust of the Tarim Basin (Robinson et al., 2004). Muztag Ata and Kongur Shan are bounded on their western flanks by an active system of strike-slip faults at the northwesternmost termination of the Karakoram Fault (Tapponnier et al., 1982; Brunel et al., 1994). East-west extension along these faults has led to the opening of pull-apart, half-graben intramontane basins (Brunel et al., 1994).

At Bulun Kol (kol means lake) (Fig. 1; 38°44′N, 75°02′E, 3310 m asl), the average annual temperature is 0.7 °C, and the mean annual precipitation is 127 mm (during 1956–1968). The highest precipitation occurs between April and May as a result of the penetration of the midlatitude westerlies into the region (Miehe et al., 2001). At Muztag Ata (Fig. 1), the mean annual precipitation to the glacier accumulation zone is ~300 mm at 5910 m asl (38°42′N, 75°01′E). Summer precipitation, which could be associated with the south Asian monsoon, accounts for <30% of the annual total. Most precipitation is therefore supplied by midlatitude westerly flow, which reaches its maximum in spring (March to May). Wake et al. (1994) found that the annual maximum particle concentrations occur at the spring dust storm period, which is coincident with the time of the peak precipitation, supplied by midlatitude westerlies. Numerous authors have suggested that glaciers in this region are likely to be more sensitive to changes in precipitation than temperature changes (Derbyshire, 1981; Shi, 2002; Owen et al., 2005). This characteristic may extend back beyond the last glacial cycle.

Skrine (1925), Fort and Peulvast (1995), Ono et al. (1997), and Seong et al. (2008) provide basic descriptions of the glacial geomorphology in the Muztag Ata and Kongur Shan region. Multiple successions of moraines occur within each valley in the forelands of Muztag Ata and Kongur Shan, together with a range of glacial and paraglacial landforms including scree cones, debris flow fans, glaciofluvial outwash terraces, alluvial fans, and floodplains (Figs. 2 and 3; Seong et al., 2008). With the exception of three radiocarbon ages on Late Glacial deposits (Ono et al., 1997), there are no numerical dates on any of the glacial landforms. Ono et al. (1997) used magnetic susceptibility in outwash terrace deposits to argue that the moraines related to the terrace deposits were formed during the penultimate glacial cycle and during at least three major glacial advances during the last glacial cycle. Using this chronology, Ono et al. (1997) reconstructed equilibrium-line altitude (ELA) depressions of ~700 m and ~100 m for the penultimate glacial and last glacial cycles, respectively. Seong et al. (2008) also calculated ELAs and ELA depressions for Muztag Ata and Kongur Shan to show the asymmetry of the massifs and to examine possible glacial controls on erosion.

METHODS

Fieldwork was undertaken to obtain a quantitative chronology for the multiple glaciations in Muztag Ata and Kongur Shan. Detailed study areas were chosen within each massif to map the glacial geology and to apply TCN dating methods. These are shown in Figures 1 and 2. We did not map moraines outside of these study area as this was beyond the scope of our study.

A common practice in glacial geology is to group moraines and associated landforms together to develop a morphostratigraphy for a region on the basis of their position in the landscape, preservation, relative weathering characteristics, type of landform association (that is usually a function of the type of glacier that produced the landforms), and/or soil development (Rose and Menzies, 1995). These groups of landforms are assigned a glacial stage name (Owen et al., 1998; Hughes et al., 2005). This allows the glacial geologist to correlate landforms assigned to the same stage throughout a region, and sometimes between regions, without inferring a numerical age for that glacial stage. Often these stages are tentatively correlated with a particular climatostratigraphic time, such as the Younger Dryas Stade. Ultimately, however, geochronological techniques are applied to determine the numerical age of the glacial stage. This allows climatic inferences to be made, and to determine other factors such as rates of paleoenvironmental change and landscape evolution. This approach is discussed in more detail in Owen et al. (1998) and Hughes et al. (2005). We adopt this approach in our study of the Muztag Ata and Kongur Shan massifs. In addition, for clarification of chronologic terms, we define the global Last Glacial Maximum (LGM) as 18–24 cal kyr B.P. (at chronozone level 2; Mix et al., 2001), the last glacial cycle to include marine oxygen isotope stages (MIS) 5d through 2, and the penultimate glacial as MIS 6. Glaciers in many mountain regions of the world reached their maximum extent earlier than the global LGM during the last glacial (Gillespie and Molnar, 1995; Thackray et al., 2008) and should be referred to as the local last glacial maximum.

No glacial stage names had been previously applied to the landforms in this region; therefore, we grouped the landforms in the study area together on the basis of morphostratigraphy, preservation, relative weathering characteristics, and type of landform association. Three distinctive sets of moraines were recognized within the region. Each set of landforms was assigned a glacial stage name, named after a nearby village. From oldest to youngest they include the Karasu, Subaxh, and Olimde glacial stages. These are discussed in detail in the glacial succession section below, and more detailed descriptions for each moraine that was dated are provided in Part A of the GSA Data Repository item[1].

Distinct moraines and/or sets of moraine ridges, that geographically separated from each other, were numbered sequentially from oldest to youngest (1 = oldest; 8 = youngest). We used the following notation, where the letter m represents a moraine or moraine set, with a subscript letter representing the valley locations (A to I, representing locations A to I in Figs. 1, 2, and 4), and a subscript number representing the relative age (1 = oldest; 8 = youngest). The youngest moraine in study area A, for example, is labeled m_{8A}. We reserve m_1 and m_2 for moraines of the Karasu

[1]GSA Data Repository Item 2008230, moraine descriptions and calculations for terrestrial cosmogenic nuclide surface-exposure ages for the Muztag Ata–Kongur Shan region of westernmost Tibet based on different scaling models, is available at www.geosociety.org/pubs/ft2008htm. Requests may also be sent to editing@geosociety.org.

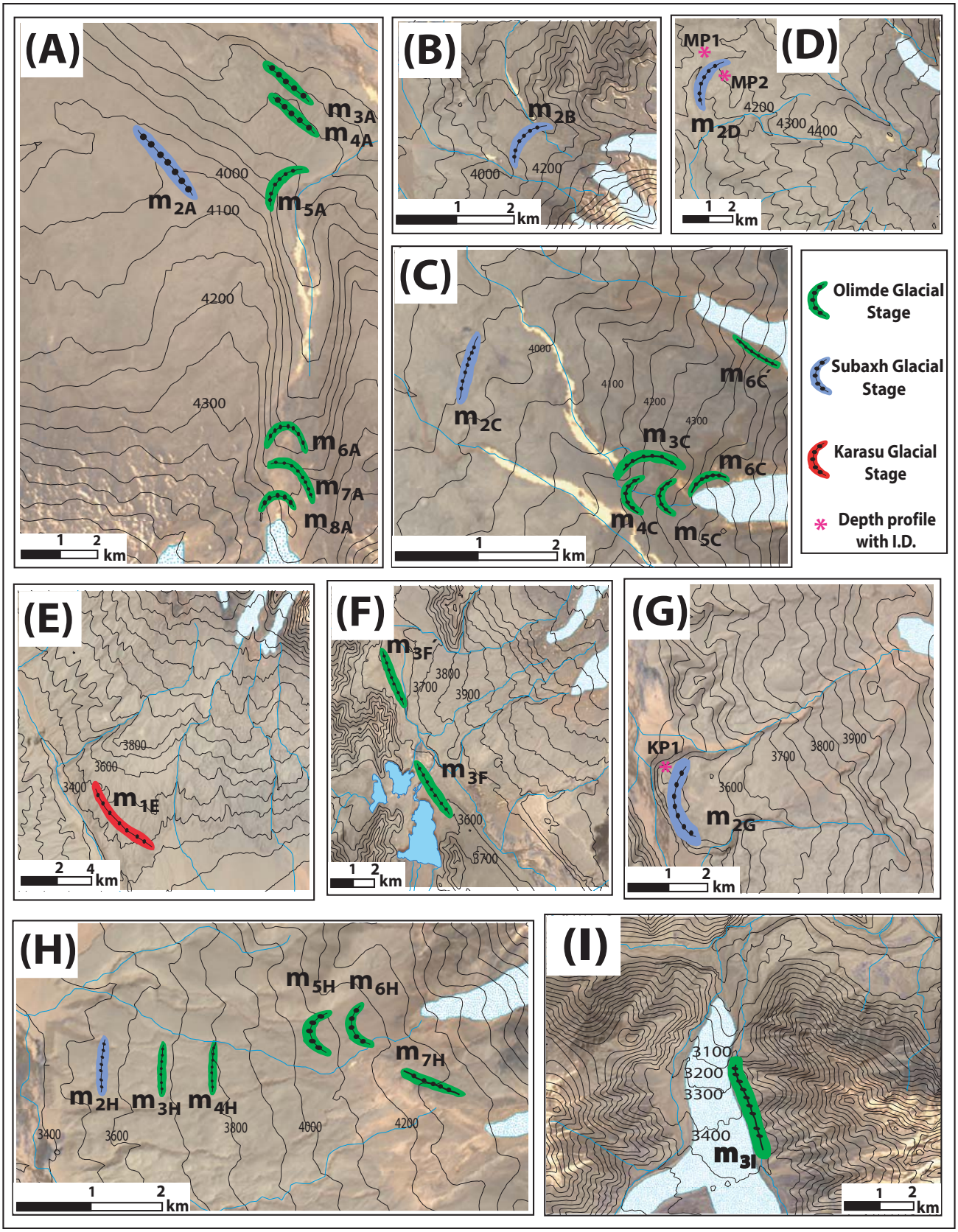

Figure 2. Advanced spaceborne thermal emission and reflection radiometer (ASTER) images (scene #: AST_L1A.003:2003030305 for Kongur Shan and AST_L1A.003:2003030307 for Muztag Ata) of the detailed study areas showing the moraines that were examined and dated using terrestrial cosmogenic nuclide (TCN) methods. Each area is shown in Figure 1.

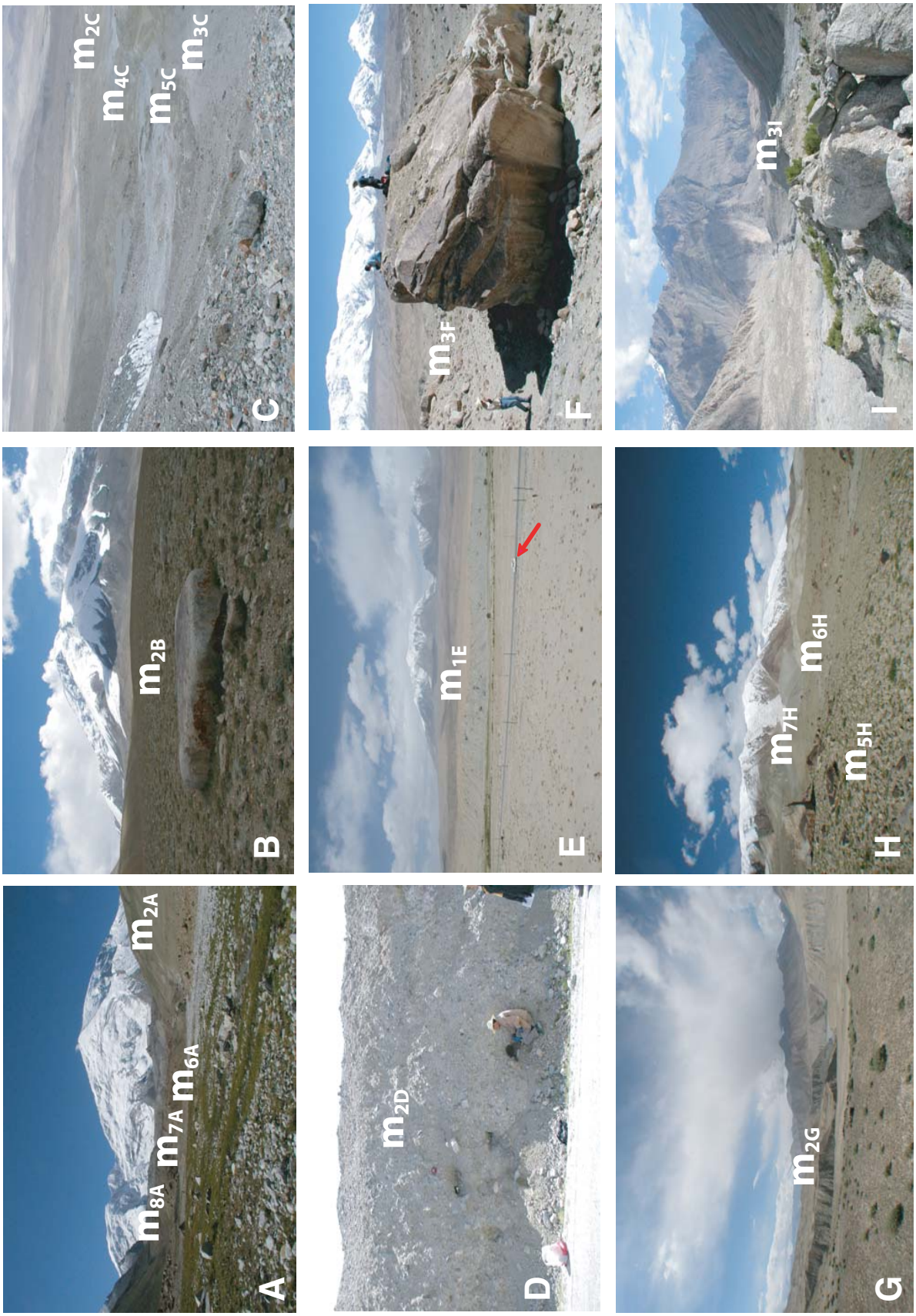

Figure 3. Glacial landforms of different ages in Muztag Ata and Kongur Shan. (A) View looking along Olimde valley at moraines m_{2A}, m_{6A}, m_{7A}, and m_{8A}. (B) Glacial boulder (~2 m in diameter) produced by piedmont glacier during the penultimate or last glacial cycle located below the Yangbuk Glacier (Subaxh glacial stage). (C) View looking down Kartamak Glacier at moraines m_{2C}, m_{3C}, m_{4C}, and m_{5C} (Olimde glacial stage). (D) View of piedmont glacial deposit of the penultimate or last glacial cycle that was sampled for a TCN surface-exposure depth-profile (Subaxh glacial stage). (E) View looking southwest of Muztag Ata at glacial deposit >100 m thick of the Karasu glacial stage. The car in the foreground provides scale. (F) Large glacial boulder (MUST-1) on the hummocky moraine formed ~8200 yr ago to the northwest of Kara Kol (Olimde glacial stage). (G) View of glacial deposits formed during the penultimate or last glacial cycle (Subaxh glacial stage). (H) View of moraines m_{5H}, m_{6H}, and m_{7H} produced by the Ting Glacier (Olimde glacial stage). (I) View of lateral moraine deposited by debris-covered Karayalak Glacier (Olimde glacial stage).

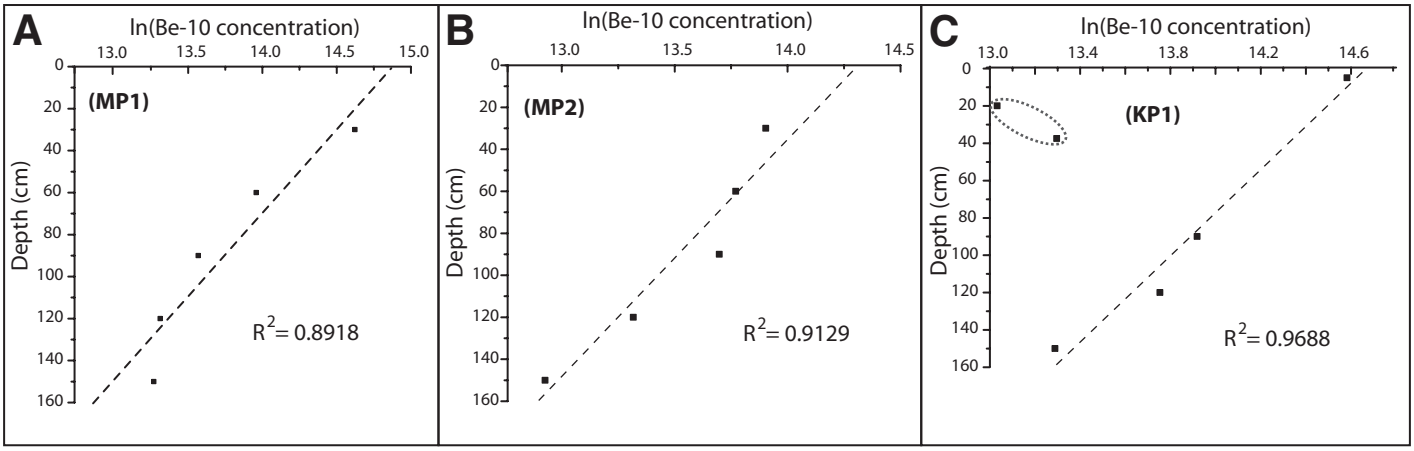

Figure 4. ^{10}Be terrestrial cosmogenic nuclide surface-exposure depth profiles within tills. Plots of $\log_e$ ^{10}Be concentrations with depth for (A) MP1, (B) MP2, and (C) KP1. Samples at 20 cm and 40 cm (within the dotted circle) for KP1 were not used in the calculation of surface concentrations.

and Subaxh glacial stages, respectively. This provided us with a framework to apply TCN surface-exposure dating that could be objectively used to compare the glacial chronologies between distant study areas of both massifs.

We used the glacial stages and relative chronologies to determine our sampling strategy for TCN surface-exposure dating. Samples weighing more than 500 g were collected from the surfaces of quartz-rich boulders, usually granite or gneiss, along moraine crests at locations where there was no apparent evidence of exhumation or slope instability. Four to seven boulders from each moraine ridge were sampled and dated to provide a check on the reproducibility of the ages and to check for the possibility of the presence of TCNs inherited from prior exposure to cosmic rays. Each boulder was photographed, measured, and the degree of weathering and the site conditions were recorded. The inclination from the boulder site to the tops of surrounding mountain ridges or peaks was measured as a function of azimuth to determine the topographic shielding. In addition, we collected depth profiles from three depositional surfaces, comprising till, that had few surface boulders. Each depth profile comprised five bulk samples weighing ~1000 g, of sand size fraction, collected between the surface and to a depth of 150 cm.

The ^{10}Be TCN surface-exposure samples were prepared in the geochronology laboratories at the University of Cincinnati. First, the samples were crushed and sieved. Quartz was then separated from the 250- to 500-µm size fraction using the methods of Kohl and Nishiizumi (1992). After addition of ^{9}Be carrier, Be was separated and purified by ion exchange chromatography and precipitated at pH >7. The hydroxides were oxidized by ignition in quartz crucibles. BeO was mixed with Nb metal and loaded into stainless steel cathodes for determination of the ^{10}Be/^{9}Be ratio by accelerator mass spectrometry at the Center for Accelerator Mass Spectrometry in the Lawrence Livermore National Laboratory. Isotope ratios were determined relative to ICN Pharmaceutical ^{10}Be standards prepared by K. Nishiizumi (Nishiizumi et al., 2007). The measured isotope ratios were converted to ^{10}Be concentrations in quartz using the total ^{9}Be in the samples and the sample weights. TCN ^{10}Be concentrations were then converted to zero-erosion exposure ages using 3% muon contribution and a production rate of 4.98 atom/gram of quartz at sea level high latitude (SLHL) and the scaling method of Stone (2000). Ages for moraines are given with one standard deviation uncertainty (e.g., 20 ka ± 1σ). The measured ^{10}Be concentrations for the depth profiles were fitted with an exponential absorption curve, which was used to extrapolate the surface ^{10}Be concentration. This, in turn, was used to determine a minimum surface-exposure age for the surface (Fig. 4).

GLACIAL GEOLOGIC EVIDENCE

The geomorphology of the contemporary glacial and associated landforms is described in Seong et al. (2008) and expanded on in the Data Repository (Part A) (see footnote 1). Numerous authors have highlighted the confusion surrounding the misidentification of glacial and nonglacial landforms and diamictons in the Himalaya and Tibet (Derbyshire, 1983; Owen, 1991; Hewitt, 1999; Benn and Owen, 2002). In particular, large landslides can easily be mistaken for moraines. Large landslides are present within the study area and are described in detail in Seong et al. (2008). We recognize this problem and use the criteria set out in the work of Owen (1991), Hewitt (1999), and Benn and Owen (2002) to help resolve issues and only sample landforms that are unequivocally moraines in this study area. Furthermore, Fort and Peulvast (1995) and Ono et al. (1997) confirm that the landforms we examined are moraines. The oldest and outermost moraines and associated landforms occur in the forelands of the massifs (Figs. 2 and 3). These were assigned to the Karasu glacial stage, with the type site located at Karasu. The moraines of the Karasu are highly degraded and denuded, and are present on till benches that contain scattered surface boulders. Sediments comprising the moraines that were sampled contained numerous boulders, which were bullet-shaped and edge-rounded with occasional striations. These are best seen in the SW foreland of Muztag Ata, ~35 km NE of the town of Kashkurgan (Figs. 2E and 3E). At this location, the Karasu glacial stage moraines comprise a giant lobe of multiple moraines ridges that rise >200 m above the foreland. Exposures in gullies along the edge of this moraine complex reveal that it is composed of massive matrix-supported diamict, which contains boulders up to 5 m in diameter. Surface boulders are sparse and some meter-size boulders are weathered flat to the surface of the landform.

Areas of moraine with numerous highly weathered surface boulders are present near the frontal slopes of the massifs and along the slope of topographic highs (Figs. 2A–2D and 3B). These were assigned to the Subaxh glacial stage. The best preserved moraines are present on a small plateau area to the NE of the Olimde valley (Fig. 2A). This area is assigned the type site for this stage. Here several subdued moraine ridges trend northeastward, and they rise

10–15 m above the surrounding surface. Surface boulders reaching 10 m in diameter are scattered on the surface of these moraines. Most of the boulders have deep (several cm-dm) weathering pits and exhibit varying degrees of exfoliation. In other study areas, such as Yangbuk (Fig. 2B), the moraines are preserved against a small topographic high (ridge) and comprise subdued ridges that have surface boulders with weathering characteristics similar to those on moraines above the Olimde valley. The moraines in the Kartamak (Fig. 2C) and Taerguo (Fig. 2D) are hummocky. The hummocks rise 10–15 m above the surrounding landscape and have slopes of between 10° and 20°. The surfaces contain inset boulders with deep (cm- to dm-size) weathering pits and are exfoliated. All the moraines comprise massive matrix-supported diamict.

Well-formed latero-frontal moraines, typical of those described by Benn and Owen (2002), that form on the margins of high-altitude, debris-covered glaciers, are present within the valleys of each massif (C, H, and I in Figs. 2 and 3). These moraines were assigned to the Olimde glacial stage after the Olimde valley on the north side of Muztag Ata, which preserves one of the best successions of moraines (Fig. 2A). This is the type area for this glacial stage. In the Olimde valley, six distinct sets of moraines are present from the snout of the Olimde Glacier with the lowest two extending into the Kengxuwar River. Each set of moraines comprises composite ridges. The youngest of these moraines, nearest to the contemporary glaciers, have sharp crests and rise several tens of meters above the valley floors. The frontal slopes of these moraines are steep, commonly exceeded 30°. Their surfaces are armored with meter-size angular to subangular boulders that show no evidence of weathering. Exposures in these moraines reveal that they comprise massive matrix-supported diamicts. Some of these moraines have become rock glacierized. The moraines downvalley of these have steep sides (commonly 20°–25°) and rise to ~50 m above the valley floor. They have abundant meter-size surface boulders, many of which have mm-size weathering pits and are slightly exfoliated. The boulders in the most distal moraines are often weathered and inset into the moraines surface. Exposures confirm that they also comprise massive matrix-supported diamicts. These characteristics are typical of moraine successions in other valleys, such as the Ting (Fig. 2H) and Kartamak (Fig. 2C) study areas. The differences between the weathering characteristics of Olimde glacial stage moraines (with the exception of those immediately adjacent to the glaciers) are not great enough to allow moraines to be correlated between valleys on the basis of morphostratigraphy.

RESULTS

The ^{10}Be concentrations that we measured (Table 1) were used to calculate model surface-exposure ages to help define the late Quaternary glacial chronology for Muztag Ata and Kongur Shan region. Good agreement of TCN surface-exposure ages among multiple samples collected on individual surfaces is observed for all the moraines that were sampled except for the very oldest surfaces (A, B, and E in Figs. 1–3 and 5). The tight clustering of young ages (<1 ka between ages) on individual surfaces shows that the inheritance of TCNs in a boulder from exposure prior to emplacement in a moraine is not significant in this region. Furthermore, the very young TCN surface-exposure ages (several hundred years) for the youngest moraines support this view. Given the stochastic nature of weathering processes, a large spread of TCN surface-exposure ages for the older deposits is not surprising. The tight clustering of TCN surface-exposure ages for the younger landforms suggests that the effects of erosion are small for samples younger than ca. 15 ka.

We can estimate the effects of erosion by using the ^{10}Be measurements for the oldest boulders (MUST 48–50 and 88–89) and assuming secular equilibrium has been reached (Lal, 1991). The measured ^{10}Be concentrations in these boulders indicate that the maximum erosion rate lies between 1 and 3 m/my. A rate of 1 m/my is consistent with rates derived from TCN data for adjacent regions (Lal, 1991; Lal et al., 2004; Owen et al., 2006) and other semiarid regions outside of the Himalayan-Tibetan orogen (e.g., Small et al., 1997; Zehfuss et al., 2001). Applying an erosion rate of 1.0 m/m.y., we find that an age of 10 ka calculated assuming zero erosion would underestimate the true age by 1%; an age of 50 ka, by 4%; an age of 100 ka, by 10%; an age of 200 ka, by 22%; and an age of 300 ka, by 42% (cf. Gosse and Phillips, 2001; Owen et al., 2006).

Currently there is much debate regarding the appropriate scaling models and geomagnetic corrections for TCN production to calculate TCN ages, especially for low-latitude and high-altitude regions (e.g., Pigati and Lifton, 2004; Staiger et al., 2007). To assess the effects of using different scaling models and geomagnetic corrections on modeled TCN ages, we calculated our TCN ages using five different schemes. The results are shown in detail in Figures DR1–3 and Table DR1 (see footnote 1). The different calculation schemes result in Holocene ages that differ by a few percent and Late Pleistocene ages that differ by as much as 10%. We use the time-constant scaling method of Lal (1991) and Stone (2000) because there is currently no agreement as to which scaling model and/or geomagnetic correction should be used to calculate ages for this latitude and altitude. Using this model, or any of the other age calculation methods, does affect our conclusions.

Corrections were not made for shielding due to snow cover. Snow shielding would systematically underestimate the effective ages. Most samples were collected from tall (>1-m-high), large (>1 m in diameter) boulders that are not usually affected by snow. Our experience has shown that snow blows off the top of tall, large boulders (cf. Owen et al., 2003c). The boulders whose upper surfaces stand high above modern snowpack would be little shielded from secondary cosmic rays, and hence this would have minimal effect on apparent age (Benson et al., 2004). Furthermore, since the region is semiarid there would be little snowpack accumulation throughout the Holocene. In addition, there is no clear relationship between boulder height and age for sets of ages, which suggests that snow cover and/or exhumation of boulders provides no systematic bias to the ages on individual moraines.

The good agreement in ages between boulders from the same moraine reinforces our conclusion that erosion has not played a significant role in altering the age estimates in moraines younger than the global LGM and reinforces our finding that moraine formation occurred during well-defined periods of glacial advance. For each of the study areas, the TCN ages on sampled moraines confirm the morphostratigraphic relationships: that is, each set of ages on each morphostratigraphically younger moraine are progressively younger than the previous moraine.

The geomorphic evidence shows that glaciation in the region became less extensive with time (Figs. 2 and 3). The style of glaciation changed from expanded ice-cap glaciation during the Karasu Glacial to piedmont glaciation during the Subaxh Glacial, ending in restricted valley glaciers during the Olimde Glacial. Using the morphostratigraphy, relative chronology, and TCN ages, we make broad correlations between the valleys studied in Muztag Ata and Kongur Shan. These are shown in Table 2.

Karasu Glacial Stage

The ice caps during this stage advanced >10 km from the present glacier limits. A good example of the glacial geologic evidence for this glacial stage can be seen at the southern portion of Muztag Ata (area E; Figs. 2 and 3). Here glacial deposits form a 10-km-wide and >150-m-thick piedmont plateau. Five boulders were dated to define the age of this surface. The TCN surface-exposure dates on boulders

TABLE 1. SAMPLING LOCATIONS FOR BOULDERS, BOULDER SIZE, SAMPLE THICKNESS, TOPOGRAPHIC SHIELDING FACTORS, ^{10}Be CONCENTRATIONS, AND ^{10}Be SURFACE EXPOSURE AGES

Sample ID	Latitude (±0.01 °N)	Longitude (±0.01 °E)	Altitude (m asl)	Shielding factor*	Boulder height/width (m)	Sample thickness (cm)	^{10}Be (10^6 atoms/g)†	^{10}Be exposure age (ka)§			Map	Moraine number	Glacial stage
								(ε = 0 m/ma)	(ε = 1 m/ma)	(ε = 3 m/ma)			
MUST-1	38.467	75.061	3689	1	7.0/8.0	5	0.501 ± 0.013	8.7 ± 0.2	8.8 ± 0.2	8.9 ± 0.2	F	m_{3F}	Olimde
MUST-2	38.467	75.062	3681	1	4.5/4.0	5	0.496 ± 0.013	8.7 ± 0.2	8.8 ± 0.2	8.9 ± 0.2	F	m_{3F}	Olimde
MUST-3	38.465	75.065	3700	1	2.8/3.0	5	0.516 ± 0.016	8.9 ± 0.3	9.0 ± 0.3	9.2 ± 0.3	F	m_{3F}	Olimde
MUST-4	38.464	75.065	3709	1	3.0/3.2	5	0.499 ± 0.013	8.6 ± 0.2	8.7 ± 0.2	8.8 ± 0.2	F	m_{3F}	Olimde
MUST-5	38.466	75.062	3688	1	3.6/1.9	5	0.490 ± 0.013	8.6 ± 0.2	8.7 ± 0.2	8.8 ± 0.2	F	m_{3F}	Olimde
MUST-6	38.467	75.061	3685	1	3.4/2.9	5	0.488 ± 0.012	8.5 ± 0.2	8.6 ± 0.2	8.7 ± 0.2	F	m_{3F}	Olimde
MUST-7	38.511	75.034	3535	1	2.5/1.0	5	0.467 ± 0.017	8.9 ± 0.3	8.9 ± 0.3	9.1 ± 0.3	F	$m_{3F'}$	Olimde
MUST-8	38.516	75.032	3534	1	4.5/2.0	5	0.457 ± 0.012	8.7 ± 0.2	8.7 ± 0.2	8.9 ± 0.2	F	$m_{3F'}$	Olimde
MUST-9	38.52	75.031	3521	1	5.0/1.5	5	0.439 ± 0.011	8.4 ± 0.2	8.5 ± 0.2	8.6 ± 0.2	F	$m_{3F'}$	Olimde
MUST-10	38.521	75.032	3517	1	3.5/1.7	5	0.408 ± 0.011	7.8 ± 0.2	7.9 ± 0.2	8.0 ± 0.2	F	$m_{3F'}$	Olimde
MUST-11	38.52	75.034	3494	1	2.7/1.6	5	0.405 ± 0.011	7.9 ± 0.2	7.9 ± 0.2	8.0 ± 0.2	F	$m_{3F'}$	Olimde
MUST-12	38.521	75.034	3490	1	8.0/1.8	5	0.424 ± 0.011	8.2 ± 0.2	8.3 ± 0.2	8.4 ± 0.2	F	$m_{3F'}$	Olimde
MUST-13	38.514	75.035	3511	1	7.0/3.0	5	0.421 ± 0.014	8.1 ± 0.3	8.1 ± 0.3	8.3 ± 0.3	F	$m_{3F'}$	Olimde
MUST-14	38.513	75.035	3521	1	3.2/1.4	5	0.428 ± 0.011	8.2 ± 0.2	8.2 ± 0.2	8.4 ± 0.2	F	$m_{3F'}$	Olimde
MUST-15	38.391	75.128	3986	1	5.4/9.1	5	8.168 ± 0.213	125.0 ± 3.4	141.2 ± 4.3	203.9 ± 10.0	A	m_{2A}	Olimde
MUST-16	38.394	75.131	3987	1	4.0/5.0	5	7.018 ± 0.162	106.9 ± 2.5	118.4 ± 3.1	157.0 ± 5.8	A	m_{2A}	Subaxh
MUST-17	38.394	75.132	3988	1	4.0/9.5	5	4.577 ± 0.106	69.1 ± 1.6	73.6 ± 1.9	85.7 ± 2.6	A	m_{2A}	Subaxh
MUST-18	38.394	75.132	3989	1	1.7/4.0	5	2.942 ± 0.069	44.1 ± 1.1	45.9 ± 1.1	50.1 ± 1.4	A	m_{2A}	Subaxh
MUST-19	38.394	75.132	3991	1	3.5/3.5	5	8.826 ± 0.201	135.0 ± 3.2	154.2 ± 4.2	235.8 ± 11.2	A	m_{2A}	Subaxh
MUST-20	38.393	75.133	4006	1	2.0/5.6	5	5.928 ± 0.188	89.0 ± 2.9	96.8 ± 3.4	120.0 ± 5.5	A	m_{2A}	Subaxh
MUST-21	38.393	75.171	3862	1	0.7/2.5	5	0.433 ± 0.011	6.9 ± 0.2	6.9 ± 0.2	7.0 ± 0.2	A	m_{5A}	Olimde
MUST-22	38.393	75.172	3864	1	2.5/2.4	5	0.405 ± 0.011	6.4 ± 0.2	6.5 ± 0.2	6.5 ± 0.2	A	m_{5A}	Olimde
MUST-23	38.393	75.172	3862	1	1.1/4.0	5	0.394 ± 0.014	6.3 ± 0.2	6.3 ± 0.2	6.4 ± 0.2	A	m_{5A}	Olimde
MUST-24	38.393	75.171	3862	1	1.0/2.5	5	0.403 ± 0.015	6.4 ± 0.2	6.4 ± 0.2	6.5 ± 0.2	A	m_{5A}	Olimde
MUST-25	38.393	75.171	3862	1	0.5/2.5	5	0.419 ± 0.011	6.7 ± 0.2	6.7 ± 0.2	6.8 ± 0.2	A	m_{5A}	Olimde
MUST-26	38.393	75.172	3861	1	0.7/3.5	5	0.422 ± 0.011	6.7 ± 0.2	6.7 ± 0.2	6.8 ± 0.2	A	m_{5A}	Olimde
MUST-27	38.364	75.171	4023	0.99	2.1/0.8	5	0.431 ± 0.013	6.4 ± 0.2	6.4 ± 0.2	6.5 ± 0.2	A	m_{6A}	Olimde
MUST-28	38.364	75.171	4024	0.99	4.8/2.9	5	0.458 ± 0.012	6.8 ± 0.2	6.8 ± 0.2	6.9 ± 0.2	A	m_{6A}	Olimde
MUST-29	38.364	75.171	4025	0.99	6.1/2.1	5	0.443 ± 0.012	6.5 ± 0.2	6.6 ± 0.2	6.6 ± 0.2	A	m_{6A}	Olimde
MUST-30	38.364	75.171	4026	0.98	5.1/1.1	5	0.467 ± 0.012	7.0 ± 0.2	7.0 ± 0.2	7.1 ± 0.2	A	m_{6A}	Olimde
MUST-31	38.363	75.171	4028	0.98	3.2/0.7	5	0.431 ± 0.011	6.4 ± 0.2	6.4 ± 0.2	6.5 ± 0.2	A	m_{6A}	Olimde
MUST-32	38.361	75.171	4082	0.99	4.1/2.0	5	0.119 ± 0.006	1.7 ± 0.1	1.7 ± 0.1	1.7 ± 0.1	A	m_{7A}	Olimde
MUST-33	38.361	75.171	4081	0.99	3.9/2.0	5	0.124 ± 0.006	1.8 ± 0.1	1.8 ± 0.1	1.8 ± 0.1	A	m_{7A}	Olimde
MUST-34	38.36	75.172	4094	0.99	5.9/3.2	5	0.129 ± 0.006	1.8 ± 0.1	1.8 ± 0.1	1.8 ± 0.1	A	m_{7A}	Olimde
MUST-35	38.359	75.172	4120	0.98	5.2/2.1	5	0.150 ± 0.006	2.1 ± 0.1	2.1 ± 0.1	2.1 ± 0.1	A	m_{7A}	Olimde
MUST-36	38.356	75.173	4167	0.99	2.0/1.2	5	0.127 ± 0.006	1.7 ± 0.1	1.7 ± 0.1	1.7 ± 0.1	A	m_{7A}	Olimde
MUST-37	38.356	75.173	4176	0.99	1.7/1.1	5	0.125 ± 0.005	1.7 ± 0.1	1.7 ± 0.1	1.7 ± 0.1	A	m_{7A}	Olimde
MUST-38	38.355	75.173	4180	0.99	3.0/1.5	5	0.124 ± 0.009	1.7 ± 0.1	1.7 ± 0.1	1.7 ± 0.1	A	m_{7A}	Olimde
MUST-39	38.353	75.171	4228	1	3.2/1.6	5	0.029 ± 0.005	0.4 ± 0.1	0.4 ± 0.1	0.4 ± 0.1	A	m_{8A}	Olimde
MUST-40	38.353	75.171	4227	1	3.3/1.9	5	0.061 ± 0.005	0.8 ± 0.1	0.8 ± 0.1	0.8 ± 0.1	A	m_{8A}	Olimde
MUST-41	38.353	75.17	4238	1	9.0/3.2	5	0.039 ± 0.004	0.5 ± 0.1	0.5 ± 0.1	0.5 ± 0.1	A	m_{8A}	Olimde
MUST-42	38.411	75.165	3719	1	4.9/3.5	5	1.009 ± 0.037	17.4 ± 0.6	17.6 ± 0.7	18.2 ± 0.7	A	m_{3A}	Olimde
MUST-43	38.411	75.165	3715	1	1.8/1.0	5	0.978 ± 0.024	16.9 ± 0.4	17.1 ± 0.4	17.6 ± 0.5	A	m_{3A}	Olimde
MUST-44	38.41	75.165	3718	1	3.2/0.9	5	1.144 ± 0.027	19.7 ± 0.5	20.0 ± 0.5	20.8 ± 0.5	A	m_{3A}	Olimde
MUST-45	38.397	75.168	3857	1	6.5/3.0	5	0.859 ± 0.021	13.7 ± 0.3	13.9 ± 0.3	14.2 ± 0.4	A	m_{4A}	Olimde
MUST-46	38.397	75.167	3861	1	1.5/0.6	5	0.871 ± 0.027	13.9 ± 0.4	14.0 ± 0.4	14.4 ± 0.5	A	m_{4A}	Olimde
MUST-47	38.397	75.167	3860	1	1.9/0.7	5	0.870 ± 0.021	13.9 ± 0.3	14.0 ± 0.3	14.4 ± 0.4	A	m_{4A}	Olimde
MUST-48	38.076	75.028	3594	1	8.1/4.5	5	18.231 ± 0.611	367.1 ± 13.4	610.4 ± 42.9	Saturated	E	m_{1E}	Karasu

(*continued*)

TABLE 1. SAMPLING LOCATIONS FOR BOULDERS, BOULDER SIZE, SAMPLE THICKNESS, TOPOGRAPHIC SHIELDING FACTORS, ^{10}Be CONCENTRATIONS, AND ^{10}Be SURFACE EXPOSURE AGES (*continued*)

Sample ID	Latitude (±0.01 °N)	Longitude (±0.01 °E)	Altitude (m asl)	Shielding factor*	Boulder height/width (m)	Sample thickness (cm)	^{10}Be (10^6 atoms/g)†	^{10}Be exposure age (ka)§			Map	Moraine number	Glacial stage
								(ε = 0 m/ma)	(ε = 1 m/ma)	(ε = 3 m/ma)			
MUST-49	38.079	75.037	3623	1	7.6/4.2	5	10.909 ± 0.121	208.5 ± 2.4	260.9 ± 3.9	Saturated	E	m_{1E}	Karasu
MUST-50	38.076	75.035	3624	1	7.8/5.1	5	13.499 ± 0.192	261.0 ± 3.9	352.7 ± 7.6	Saturated	E	m_{1E}	Karasu
MUST-88	38.066	75.041	3557	1	4.8/2.1	5	7.739 ± 0.115	151.5 ± 2.3	176.4 ± 3.2	303.3 ± 11.8	E	m_{1E}	Karasu
MUST-89	38.066	75.035	3537	1	4.8/2.1	5	7.899 ± 0.215	156.4 ± 6.0	183.1 ± 8.3	329.2 ± 35.0	E	m_{1E}	Karasu
MUST-52	38.285	75.023	4580	1	5.8/4.1	5	0.013 ± 0.004	0.1 ± 0.0	0.1 ± 0.0	0.1 ± 0.0	C	m_{6C}	Olimde
MUST-53	38.285	75.026	4568	1	5.8/4.0	5	0.032 ± 0.004	0.4 ± 0.0	0.4 ± 0.0	0.4 ± 0.0	C	m_{6C}	Olimde
MUST-54	38.287	75.024	4524	1	1.1/0.5	5	0.025 ± 0.005	0.3 ± 0.0	0.3 ± 0.1	0.3 ± 0.1	C	m_{6C}	Olimde
MUST-55	38.287	75.025	4504	1	3.2/1.8	5	0.048 ± 0.005	0.6 ± 0.1	0.6 ± 0.1	0.6 ± 0.1	C	m_{6C}	Olimde
MUST-56	38.287	75.025	4511	1	1.2/0.8	5	0.041 ± 0.005	0.5 ± 0.1	0.5 ± 0.1	0.5 ± 0.1	C	m_{6C}	Olimde
MUST-57	38.288	75.013	4357	1	6.5/3.2	5	1.137 ± 0.027	14.1 ± 0.3	14.3 ± 0.4	14.6 ± 0.4	C	m_{3C}	Olimde
MUST-58	38.289	75.011	4313	1	1.3/1.1	5	1.083 ± 0.026	13.7 ± 0.3	13.9 ± 0.3	14.2 ± 0.4	C	m_{3C}	Olimde
MUST-59	38.289	75.011	4308	1	2.8/1.5	5	1.074 ± 0.034	13.6 ± 0.4	13.8 ± 0.4	14.1 ± 0.5	C	m_{3C}	Olimde
MUST-60	38.289	75.011	4300	1	1.9/0.9	5	0.993 ± 0.024	12.7 ± 0.3	12.8 ± 0.3	13.1 ± 0.3	C	m_{3C}	Olimde
MUST-61	38.289	75.008	4284	1	3.2/1.6	5	1.144 ± 0.027	14.7 ± 0.4	14.9 ± 0.4	15.3 ± 0.4	C	m_{3C}	Olimde
MUST-62	38.301	74.984	4005	1	3.1/1.3	5	1.175 ± 0.046	17.4 ± 0.7	17.7 ± 0.7	18.3 ± 0.8	C	m_{2C}	Olimde
MUST-63	38.301	74.983	4001	1	1.8/0.7	5	1.676 ± 0.045	24.9 ± 0.7	25.5 ± 0.7	26.7 ± 0.8	C	m_{2C}	Subaxh
MUST-64	38.302	74.969	3987	1	1.4/0.8	5	1.547 ± 0.037	23.2 ± 0.6	23.7 ± 0.6	24.7 ± 0.6	C	m_{2C}	Subaxh
MUST-65	38.303	74.979	3979	1	4.2/2.5	5	4.953 ± 0.093	75.4 ± 1.4	80.9 ± 1.7	96.0 ± 2.4	C	m_{2C}	Subaxh
MUST-66	38.302	74.98	3995	1	2.8/1.1	5	3.266 ± 0.056	49.0 ± 0.9	51.3 ± 0.9	56.7 ± 1.2	C	m_{2C}	Subaxh
MUST-86	38.283	74.98	3988	1	3.5/2.8	5	1.585 ± 0.038	23.8 ± 0.6	24.3 ± 0.6	25.4 ± 0.7	C	m_{2C}	Subaxh
MUST-67	38.288	75.008	4246	1	1.2/0.8	5	1.049 ± 0.034	13.7 ± 0.5	13.9 ± 0.5	14.3 ± 0.5	C	m_{4C}	Olimde
MUST-68	38.288	75.008	4244	1	3.9/1.5	5	1.027 ± 0.025	13.5 ± 0.3	13.6 ± 0.3	14.0 ± 0.4	C	m_{4C}	Olimde
MUST-69	38.287	75.007	4234	1	4.2/2.9	5	1.078 ± 0.026	14.2 ± 0.3	14.4 ± 0.4	14.8 ± 0.4	C	m_{4C}	Olimde
MUST-70	38.288	75.007	4244	1	3.5/2.1	5	1.021 ± 0.026	13.4 ± 0.3	13.5 ± 0.3	13.9 ± 0.4	C	m_{4C}	Olimde
MUST-71	38.288	75.008	4248	1	2.1/1.7	5	1.037 ± 0.026	13.6 ± 0.3	13.7 ± 0.3	14.1 ± 0.4	C	m_{4C}	Olimde
MUST-72	38.287	75.011	4295	1	1.3/1.2	5	0.892 ± 0.022	11.4 ± 0.3	11.5 ± 0.3	11.7 ± 0.3	C	m_{5C}	Olimde
MUST-73	38.286	75.011	4298	1	2.0/1.1	5	0.770 ± 0.019	9.8 ± 0.2	9.9 ± 0.3	10.1 ± 0.3	C	m_{5C}	Olimde
MUST-74	38.286	75.011	4292	1	3.2/1.4	5	0.807 ± 0.020	10.3 ± 0.3	10.4 ± 0.3	10.6 ± 0.3	C	m_{5C}	Olimde
MUST-75	38.286	75.011	4293	1	1.5/1.2	5	0.820 ± 0.032	10.5 ± 0.4	10.6 ± 0.4	10.8 ± 0.4	C	m_{5C}	Olimde
MUST-76	38.292	75.025	4477	0.99	3.4/1.5	5	0.399 ± 0.009	4.7 ± 0.1	4.7 ± 0.1	4.7 ± 0.1	C	$m_{6C'}$	Olimde
MUST-77	38.292	75.025	4473	0.99	2.3/1.2	5	0.337 ± 0.010	4.0 ± 0.1	4.0 ± 0.1	4.0 ± 0.1	C	$m_{6C'}$	Olimde
MUST-78	38.293	75.024	4461	0.99	3.6/1.1	5	0.353 ± 0.010	4.2 ± 0.1	4.2 ± 0.1	4.2 ± 0.1	C	$m_{6C'}$	Olimde
MUST-79	38.293	75.025	4473	0.99	2.1/0.9	5	0.336 ± 0.010	4.0 ± 0.1	4.0 ± 0.1	4.0 ± 0.1	C	$m_{6C'}$	Olimde
MUST-80	38.34	75.022	4181	1	3.8/3.2	5	2.963 ± 0.079	40.3 ± 1.1	41.8 ± 1.2	45.2 ± 1.4	B	m_{2B}	Subaxh
MUST-81	38.342	75.021	4181	1	1.2/1.2	5	1.954 ± 0.046	26.5 ± 0.6	27.1 ± 0.7	28.5 ± 0.7	B	m_{2B}	Subaxh
MUST-82	38.34	75.021	4168	1	4.3/1.5	5	5.717 ± 0.069	78.9 ± 1.0	85.0 ± 1.1	102.0 ± 1.7	B	m_{2B}	Subaxh
MUST-83	38.342	75.015	4123	1	2.2/0.8	5	1.572 ± 0.047	21.9 ± 0.7	22.4 ± 0.7	23.3 ± 0.8	B	m_{2B}	Subaxh
MUST-84	38.342	75.014	4113	1	2.2/1.2	5	4.290 ± 0.075	60.7 ± 1.1	64.2 ± 1.2	73.0 ± 1.6	B	m_{2B}	Subaxh
MUST-90	38.34	75.017	4126	1	1.5/0.6	5	7.927 ± 0.117	112.7 ± 1.7	125.7 ± 21	171.0 ± 4.3	B	m_{2B}	Subaxh
MUST-91	38.343	75.013	4117	1	1.2/0.6	5	1.784 ± 0.044	25.0 ± 0.6	25.5 ± 0.7	26.8 ± 0.7	B	m_{2B}	Subaxh
MUST-92	38.342	75.014	4117	1	0.8/0.8	5	4.629 ± 0.158	65.4 ± 2.3	69.5 ± 2.6	80.1 ± 3.5	B	m_{2B}	Subaxh
MUST-P1	38.276	74.917	4091	0.92	Depth profile	Depth profile	0.595 ± 0.015	53.1 ± 1.4	56.0 ± 1.5	7.7 ± 1.8	D	m_{2D}	Subaxh
MUST-P2	38.276	74.917	4091	0.92	Depth profile	Depth profile	0.405 ± 0.015	65.6 ± 1.6	69.7 ± 2.6	80.7 ± 3.6	D	m_{2D}	Subaxh
KONG_1	38.64	74.99	3480	1	2.2/2.1	5	0.758 ± 0.019	14.8 ± 0.4	15.0 ± 0.4	15.4 ± 0.4	H	m_{2H}	Subaxh
KONG_2	38.641	74.994	3502	1	1.7/0.9	5	1.328 ± 0.031	25.7 ± 0.6	26.3 ± 0.6	27.6 ± 0.7	H	m_{2H}	Subaxh
KONG_3	38.642	74.994	3527	1	3.2/1.5	5	0.916 ± 0.023	17.4 ± 0.4	17.7 ± 0.5	18.3 ± 0.5	H	m_{2H}	Subaxh
KONG_4	38.642	74.994	3527	1	2.9/1.5	5	1.528 ± 0.037	29.2 ± 0.7	29.9 ± 0.7	31.6 ± 0.8	H	m_{2H}	Subaxh
KONG_5	38.642	74.995	3539	1	5.1/1.7	5	0.588 ± 0.016	11.1 ± 0.3	11.2 ± 0.3	11.4 ± 0.3	H	m_{3H}	Olimde

(*continued*)

TABLE 1. SAMPLING LOCATIONS FOR BOULDERS, BOULDER SIZE, SAMPLE THICKNESS, TOPOGRAPHIC SHIELDING FACTORS, ^{10}Be CONCENTRATIONS, AND ^{10}Be SURFACE EXPOSURE AGES (*continued*)

Sample ID	Latitude (±0.01 °N)	Longitude (±0.01 °E)	Altitude (m asl)	Shielding factor*	Boulder height/width (m)	Sample thickness (cm)	^{10}Be (10^6 atoms/g)†	^{10}Be exposure age (ka)§			Map	Moraine number	Glacial stage
								(ε = 0 m/ma)	(ε = 1 m/ma)	(ε = 3 m/ma)			
KONG_6	38.642	74.995	3539	1	3.1/1.7	5	0.594 ± 0.016	11.2 ± 0.3	11.3 ± 0.3	11.6 ± 0.3	H	m_{3H}	Olimde
KONG_7	38.642	74.995	3542	1	8.0/6.5	5	0.604 ± 0.016	11.4 ± 0.3	11.5 ± 0.3	11.7 ± 0.3	H	m_{3H}	Olimde
KONG_8	38.64	75.003	3639	0.98	2.0/1.3	5	0.371 ± 0.011	6.8 ± 0.2	6.8 ± 0.2	6.9 ± 0.2	H	m_{4H}	Olimde
KONG_9	38.64	75.004	3637	0.98	9.7/8.1	5	0.366 ± 0.011	6.7 ± 0.2	6.7 ± 0.2	6.8 ± 0.2	H	m_{4H}	Olimde
KONG_10	38.64	75.004	3638	0.98	7.9/6.5	5	0.374 ± 0.011	6.8 ± 0.2	6.9 ± 0.2	6.9 ± 0.2	H	m_{4H}	Olimde
KONG_11	38.641	75.004	3639	0.98	3.5/2.1	5	0.372 ± 0.012	6.8 ± 0.2	6.8 ± 0.2	6.9 ± 0.2	H	m_{4H}	Olimde
KONG_12	38.641	75.004	3641	0.98	2.1/1.2	5	0.382 ± 0.011	7.0 ± 0.2	7.0 ± 0.2	7.1 ± 0.2	H	m_{4H}	Olimde
KONG_13	38.641	75.004	3652	0.98	3.1/2.1	5	0.373 ± 0.018	6.7 ± 0.3	6.8 ± 0.3	6.9 ± 0.3	H	m_{4H}	Olimde
KONG_14	38.644	75.041	4168	1	2.1/1.8	5	0.106 ± 0.011	1.4 ± 0.1	1.4 ± 0.1	1.4 ± 0.1	H	m_{7H}	Olimde
KONG_15	38.644	75.04	4178	1	1.2/0.9	5	0.057 ± 0.010	0.8 ± 0.1	0.8 ± 0.1	0.8 ± 0.1	H	m_{7H}	Olimde
KONG_16	38.644	75.04	4179	1	2.2/1.4	5	0.104 ± 0.010	1.4 ± 0.1	1.4 ± 0.1	1.4 ± 0.1	H	m_{7H}	Olimde
KONG_17	38.643	75.039	4178	1	1.7/1.6	5	0.088 ± 0.011	1.2 ± 0.1	1.2 ± 0.1	1.2 ± 0.1	H	m_{7H}	Olimde
KONG_18	38.649	75.032	4057	1	3.2/1.7	5	0.247 ± 0.008	3.5 ± 0.1	3.5 ± 0.1	3.6 ± 0.1	H	m_{5H}	Olimde
KONG_19	38.649	75.032	4057	1	3.4/1.8	5	0.240 ± 0.009	3.4 ± 0.1	3.4 ± 0.1	3.5 ± 0.1	H	m_{5H}	Olimde
KONG_20	38.649	75.032	4060	1	3.7/1.2	5	0.235 ± 0.009	3.3 ± 0.1	3.4 ± 0.1	3.4 ± 0.1	H	m_{5H}	Olimde
KONG_21	38.645	75.031	4039	1	2.4/1.3	5	0.060 ± 0.006	0.9 ± 0.1	0.9 ± 0.1	0.9 ± 0.1	H	m_{5H}	Olimde
KONG_22	38.645	75.031	4042	1	2.7/1.2	5	0.314 ± 0.010	4.5 ± 0.1	4.5 ± 0.1	4.6 ± 0.1	H	m_{5H}	Olimde
KONG_23	38.644	75.028	4008	1	2.3/1.1	5	0.195 ± 0.008	2.8 ± 0.1	2.9 ± 0.1	2.9 ± 0.1	H	m_{6H}	Olimde
KONG_24	38.643	75.028	4005	1	2.3/1.4	5	0.101 ± 0.007	1.5 ± 0.1	1.5 ± 0.1	1.5 ± 0.1	H	m_{6H}	Olimde
KONG_25	38.645	75.026	3999	1	6.1/2.3	5	0.224 ± 0.007	3.3 ± 0.1	3.3 ± 0.1	3.3 ± 0.1	H	m_{6H}	Olimde
KONG_26	38.645	75.026	3997	1	3.2/2.1	5	0.224 ± 0.008	3.3 ± 0.1	3.3 ± 0.1	3.3 ± 0.1	H	m_{6H}	Olimde
KONG_27	38.646	75.026	4000	1	1.7/1.2	5	0.157 ± 0.008	2.3 ± 0.1	2.3 ± 0.1	2.3 ± 0.1	H	m_{6H}	Olimde
KONG_28	38.646	75.026	4000	1	2.1/0.6	5	0.077 ± 0.006	1.1 ± 0.1	1.1 ± 0.1	1.1 ± 0.1	H	m_{6H}	Olimde
KONG_29	38.593	75.01	3573	1	5.1/3.2	5	1.566 ± 0.042	29.2 ± 0.8	29.9 ± 0.8	31.6 ± 0.9	G	m_{2G}	Subaxh
KONG_30	38.595	75.003	3554	1	3.7/1.9	5	3.023 ± 0.071	57 ± 1.4	60.3 ± 1.5	68.0 ± 1.9	G	m_{2G}	Subaxh
KONG_P1	38.594	74.995	3541	0.99	Depth profile	Depth profile	2.154 ± 0.054	35.3 ± 0.9	36.0 ± 1.1	37.6 ± 1.2	G	m_{2G}	Subaxh
KONG_31	38.701	75.284	3350	1	3.5/2.8	5	N.A.				I	m_{3I}	
KONG_32	38.701	75.267	3347	1	3.1/2.4	5	N.A.				I	m_{3I}	
KONG_33	38.701	75.267	3349	1	2.4/1.8	5	N.A.				I	m_{3I}	
KONG_34	38.704	75.282	3331	1	2.8/1.7	5	N.A.				I	m_{3I}	
KONG_35	38.709	75.28	3326	0.93	3.2/1.4	5	0.034 ± 0.006	0.8 ± 0.1	0.8 ± 0.1	0.8 ± 0.1	I	m_{3I}	Olimde
KONG_36	38.709	75.28	3328	0.93	7.2/3.1	5	0.059 ± 0.007	1.3 ± 0.2	1.3 ± 0.2	1.3 ± 0.2	I	m_{3I}	Olimde
KONG_37	38.711	75.28	3309	0.93	4.2/2.2	5	0.063 ± 0.006	1.5 ± 0.1	1.5 ± 0.1	1.5 ± 0.1	I	m_{3I}	Olimde
KONG_38	38.714	75.28	3299	0.93	7.3/3.1	5	0.039 ± 0.007	0.9 ± 0.2	0.9 ± 0.2	0.9 ± 0.2	I	m_{3I}	Olimde
KONG_39	38.736	75.273	3125	0.93	4.1/1.7	5	N.A.				I	m_{3I}	
KONG_40	38.737	75.273	3125	0.93	4.8/3.4	5	N.A.				I	m_{3I}	
KONG_41	38.738	75.273	3118	0.93	2.8/2.2	5	0.014 ± 0.005	0.4 ± 0.1	0.4 ± 0.1	0.4 ± 0.1	I	m_{3I}	Olimde

Note: Minimum ^{10}Be ages were calculated using Stone (2000) scaling factors; sea-level high-latitude (SLHL) production rate = 4.98 ^{10}Be atoms/g quartz per year; and sample thickness of 5 cm. MP1, MP2, and KP1 are depth profile samples shown in Figure 4; asl—above sea level. All the ages are uncorrected for change in geomagnetic effects.

*Shielding factor as calculated to correct for topographic barriers using the methods of Nishiizumi et al. (1989).

†Atoms of ^{10}Be per gram of quartz before application of shielding correction factor.

§Uncertainty is cited as analytical errors.

N.A.—not available. It may be due to little concentration of ^{10}Be in the rock sampled and thus out of range for detection limit of ^{10}Be/^{9}Be ($<10^{-16}$) in accelerator mass spectrometry.

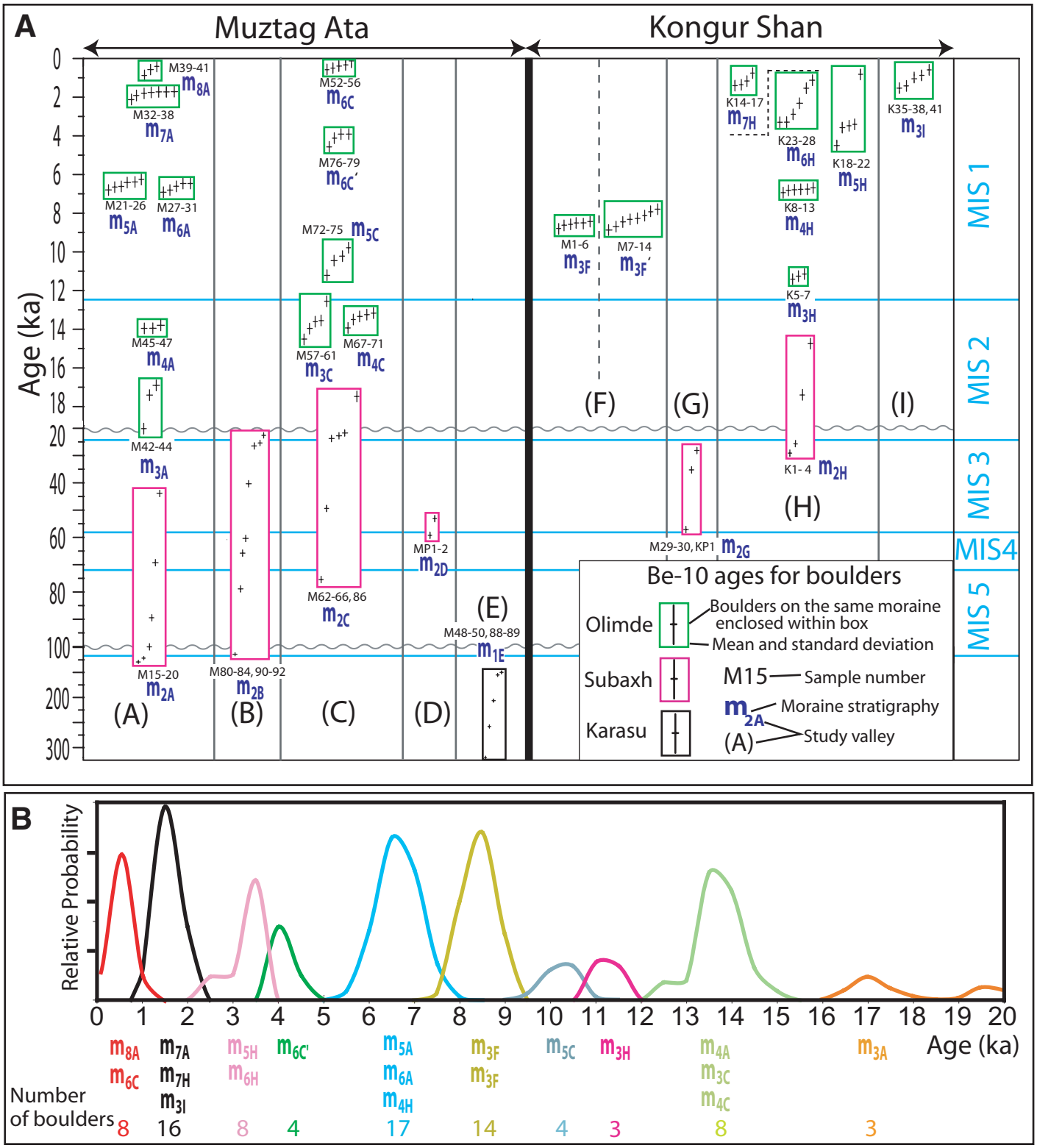

Figure 5. ^{10}Be terrestrial cosmogenic nuclide surface-exposure ages for boulders on moraines dated from each of the study areas. (A) Individual ^{10}Be TCN surface-exposure ages plotted for each region. Marine oxygen-isotope stages (MIS) are shown in light blue. Note that the vertical scale changes at 20 ka and 100 ka (marked by the light-gray undulating lines). The error bars are for analytical uncertainty. (B) Probability distributions for ^{10}Be TCN surface-exposure ages grouped per each glacial advance over the past 20,000 yr (Olimde glacial stage). Every ^{10}Be TCN surface-exposure age for each advance was converted to a probability distribution and summed to show the relative potential of the ages of each advance. Each different color represents a distinct glacial advance.

TABLE 2. CORRELATION OF THE MORAINES BETWEEN THE VALLEYS OF THE STUDY REGION

Ages	Valleys								
	A	B	C	D	E	F	G	H	I
Several hundred years (Little Ice Age)	m_{8A}		m_{8C}						
1.4 ± 0.3 ka	m_{7A}							m_{7H}	m_{3I}
3.3 ± 0.6 ka								m_{6H} and m_{5H}	
4.2 ± 0.3 ka			$m_{6C'}$						
6.7 ± 0.2 ka	m_{6A} and m_{5A}							m_{4H}	
8.4 ± 0.4 ka						m_{3F} and $m_{3F'}$			
10.2 ± 0.3 ka			m_{5C}						
11.2 ± 0.1 ka								m_{3H}	
13.7 ± 0.5 ka	m_{4A}		m_{4C} and m_{3C}						
17.1 ± 0.3 ka	m_{3A}								
Last glacial cycle or penultimate glacial cycle	m_{2A}	m_{2B}	m_{2C}	m_{2D}			m_{2G}	m_{2H}	
Pre-penultimate glacial cycle					m_{1E}				

Note: m—moraine. Numbers 1–8 are for relative age (1—oldest moraine; 8—youngest); subscript letters (a–i) indicate the location of the detailed study areas (A–I). Uncertainties are 1 standard deviation.

span between 151 and 367 ka (M_{1E}; Fig. 5A). Although there is a large spread of ages, which suggests the youngest ages represent significant erosion and or exhumation of boulders, we have broadly assigned the landform to a glaciation prior to the penultimate glacial cycle.

Subaxh Glacial Stage

Glaciers during this stage formed subdued end and lateral moraines, and hummocky moraines delimiting the extent of piedmont glaciers (Table 1 and Fig. 1). Boulders from this stage have TCN surface-exposure ages ranging from >100 ka to 15 ka. Six surfaces were dated for age control for this glacial stage. This included six boulders from Olimde glacier (A in Figs. 2 and 3) on the oldest surface (m_{2A}), providing ages ranging between 44 and 134 ka. In addition, ages for eight boulders from the surface below Yangbuk glacier (B in Figs. 2 and 3) range between 21 and 112 ka. Considering the possible problems associated with inheritance and erosion, this landform probably represents a glacial advance that occurred during the early part of the last glacial cycle, possibly during MIS 3 and/or MIS 4. In the Kartamak valley (C in Figs. 1–3) our dating shows that the Kartamak glacier (m_{2C}) advanced between ca. 17 and 75 ka. The advancing glaciers likely converged to form a broad, lobate, piedmont glacier. The ages on these landforms are scattered and may reflect some inheritance (the oldest ages) of TCNs and postdepositional erosion (the youngest ages). If ages beyond two standard deviations of the mean of the ages are rejected (specifically MUST-62), the dating suggests that this glacial stage probably represents a glacial advance that occurred during early MIS 3 or late MIS 2. Two boulders and one depth profile were dated in Kokodak valley on m_{2G} (G in Figs. 2 and 3). The TCN surface-exposure ages range between 29 and 57 ka suggesting that these formed during MIS 3. Four boulders were dated from hummocky moraines that occur farthest from the Ting glacier valley (m_{2H}). These date to between 14 and 29 ka. Despite the scatter of ages, considering effects of erosion, these ages suggest that this landform might have formed during the global LGM.

The two depth profiles that were examined in till in the Taerguo study area provide modeled ages for these surfaces of 53 and 67 ka (D in Figs. 2 and 3; A and B in Fig. 4). The depth-profile data show little evidence of inheritance, with the lowest (150-cm-deep) samples in the depth profile having concentrations that are 4%–5% that of surface concentrations. We cannot rule out the possibility that the surfaces where the depth profiles were examined have not been eroded, and we therefore consider these ages to be minimum values for the age of these deposits. The depth profiles support the view that this glacial stage should be assigned to the early part of the last glacial cycle.

The spread of age data for this glacial stage might reflect the local topography, since gentler sloping terrain would not allow glacial advances to be widely separated geographically, and boulders from earlier glacial deposits might be mixed in with the newly transported and deposited boulders. Sampling might, therefore, include boulders from several glacial advances and thus it is difficult to assign accurate ages to glacial advances during this glacial stage. Landforms assigned to this glacial stage likely represent multiple glacial advances during the penultimate glacial cycle and/or the last glacial cycle. Given the large scatter of ages on each landform it is difficult to precisely and accurately assign each landform to a specific time during the last two glacial cycles and/or correlate between the landforms within the two massifs and different valleys.

Olimde Glacial Stage

For each of the study areas we examined that contain landforms of the Olimde glacial stage, the TCN ages on morphostratigraphically younger moraines are progressively younger. This provides confidence in the TCN surface-exposure dating. However, the ages based on the TCN surface-exposure dating of similarly numbered moraines differ between different valleys (Fig. 5A and Table 2). This might be the result of asynchronous glaciation. Given that glacier retreat in high-mountain environments usually produces hummocky moraines in dead ice zones and do not form well-developed latero-frontal moraines (Benn and Owen, 2002; Zech et al., 2005a), we argue that the moraines sampled formed during distinct glacial advances. Alternatively, this might be a function of irregular preservation of moraines. For example, in some valleys younger glacier advances might have overridden older moraines, destroying the evidence for older advances. Given that some moraines (e.g., m_{5A}, m_{6A}, and m_{4H} and m_{4A}, m_{3C}, and m_{4C}) have the same ages (with tight clustering of boulders ages on the moraines), we favor the latter explanation, and suggest any evident asynchronicity between advances in different valleys is apparent rather than real. The tight clustering of boulder ages on moraines suggests that glaciers advanced at ca. 17.1 ka, 13.7 ka, 11.2 ka, 10.2 ka, 8.4 ka, 6.7 ka, 4.2 ka, 3.3 ka, 1.4 ka, and a few hundred years ago. Figure 5B shows the probability distributions for each of these glacial advances.

Three boulders from one latero-frontal moraine belonging to this stage were dated and define a 17.1 ± 0.3 ka glacial advance (area A in Fig. 1 and m_{3A} in Fig. 2). The TCN surface-exposure ages range between 16.8 and 19.6 ka, with reasonable clustering at ca. 17.1 ka. The

oldest age (19.3 ka) for this moraine is older than the younger of m_{2H} and m_{2C}, but the style of glaciation of m_{3A} (latero-frontal moraine) is different from m_{2H} and m_{2C}, which are hummocky moraines, suggesting that this boulder may have been reworked from an older deposit and thus may contain inherited ^{10}Be due to prior exposure from a moraine that formed during the Subaxh glacial stage. Despite the small number of samples, two out of three show agreement at ca. 17.1 ka (16.8 and 17.3 ka). Therefore, it is likely that this event occurred during the Late Glacial at ca. 17.1 ± 0.3 ka.

There are three sets of latero-frontal moraines that define a 13.7 ka glacial advance. Three boulders were dated in the Olimde valley (13.8 ± 0.1 ka; Fig. 1; m_{4A} in Fig. 2), and five boulders each (13.7 ± 0.7 ka; m_{3C} and 13.6 ± 0.3 ka; m_{4C}) from two moraines in the Kartamak valley. Each moraine has TCN surface-exposure ages that tightly cluster around 13.7 ± 0.4 ka. Given the tight clustering of TCN surface-exposure ages and the morphostratigraphy, and the style of glaciation, we consider these moraines were produced by synchronous glacial advances. The more extensive advance in the Olimde valley compared with that for the Kartamak valley is a function of the large glaciers on the eastern and northern sides of Muztag Ata. Furthermore, the ELA depression for each valley is slightly different (260 m and 320 m for the Kartamak and Olimde valley, respectively) and is a function of the basin hypsometry, aspect, headwall geometry, and snow avalanche supply. The complexities controlling ELA in high mountains and specifically the Himalaya and Tibet are discussed in depth in Benn and Lehmkuhl (2000) and Owen and Benn (2005), and are discussed in more detail in Seong et al. (2008).

Three boulders were dated from a moraine (m_{3H}) of the Ting valley that defines an 11.2 ka glacial advance. The ages tightly cluster at 11.2 ± 0.1 ka.

TCN surface-exposure ages for four boulders on a latero-frontal moraine (m_{5C}) in Olimde valley define a glacial advance at 10.2 ka. However, there is one older age (MUST-72 at 11.3 ± 0.2 ka), which may be the result of the boulder derived from an old deposit that had TCNs from prior exposure. Given the errors associated with TCN surface-exposure dating, the possibility that this event occurred at the same advance that produced m_{3H} cannot be ruled out. In that case, the moraine age would be 10.2 ± 0.3 ka.

Two sets of moraines, each originating from ice that advanced from separate but adjacent valleys, on the southwestern slopes of Kongur Shan (F in Figs. 1 and 2) have ages that cluster around 8.7 ± 0.1 ka (m_{3F}) and 8.3 ± 0.3 ka ($m_{3F'}$). These likely define a ca. 8.4 ± 0.4 ka glacial advance. The older ages were obtained from the boulders on the hummocky moraines deposited by Kongurjiubie glacier (Fig. 1) and the younger ages from the latero-frontal moraine formed by Jangmanjiar glacier (Fig. 1). The two glaciers are adjacent and probably converged during this event.

It is noteworthy that the extensive glacier advances and corresponding ELA depression in these regions during this time were significantly greater than for any Holocene glacial advance from Muztag Ata and for Holocene glacial advances on the northwestern slopes of Muztag Ata (Ting study area; H in Figs. 1 and 2). As discussed above, the difference in ELA depression might reflect differences in basin hypsometry and aspect.

Three sets of moraines define a ca. 6.7 ± 0.2 ka glacial advance. Two of these occur in the Olimde valley and have ages that tightly cluster around 6.5 ± 0.2 ka (m_{5A}) and 6.6 ± 0.2 ka (m_{6A}). In addition, a hummocky moraine from Ting valley (Fig. 1) yields an age of 6.8 ± 0.1 ka (m_{4H}). The tight clustering of TCN surface-exposure ages suggests that exhumation and weathering of the boulders are not significant and that our ages are reasonable estimates of the true age of the moraines.

Four boulders from a terminal moraine ($m_{6C'}$) in the Kartamak valley have TCN surface-exposure ages that define a 4.2 ± 0.3 ka glacial advance.

Two sets of moraines define a 3.3 ± 0.6 ka glacial advance in the Ting valley. The TCN surface-exposure ages range from 3.7 ± 0.5 ka (m_{5H}; age for Kong_21 omitted) to 2.9 ± 0.4 ka (m_{6H}; age for Kong 24 and 28 omitted). Samples Kong_21, Kong_24, and Kong_28 have significantly younger ages than the rest of the population. These may be due to erosion or postdepositional toppling of the sampled boulder.

Three sets of moraines define a glacial advance at 1.4 ± 0.1 ka. These include TCN surface-exposure ages on seven boulders from the terminal moraine of Olimde glacier (m_{7A}), four boulders from Ting glacier (m_{7H}), and seven samples from a debris-covered glacier (m_{3I}) in the Karayaylak valley (Fig. 1). Ages of each moraine cluster around 1.8 ± 0.1 ka, 1.3 ± 0.1 ka (sample Kong_15 rejected), and 1.4 ± 0.1 ka (Kong_41 rejected). Samples Kong_15 and Kong_41 have significantly younger ages than the rest of the population, probably resulting from postdepositional toppling.

Fresh, sharp-crested moraines in the Olimde and Kartamak valleys dated to 0.5 ± 0.2 ka (m_{8A}) and 0.3 ± 0.1 ka (m_{6C}). These define the youngest glacial advance.

DISCUSSION

Our TCN surface-exposure dating provides the first numerically defined chronology for Muztag Ata and Kongur Shan. The oldest glacial stage, the Karasu, has ^{10}Be TCN surface-exposure ages that suggest that the moraines of this stage formed during the penultimate or earlier glacial cycles. Most of the boulders on the moraine of the Karasu glacial stage that were dated, on the southwest portion of Muztag Ata (E in Figs. 2 and 3), were intensively weathered. Given the effect of weathering, these ^{10}Be TCN surface-exposure ages must be considered to be absolute minimum ages. The wide scatter of ages does not allow us to assign this moraine to a specific marine oxygen-isotope stage. This moraine is one of the oldest in the Himalayan-Tibetan orogen and likely formed during or prior to the penultimate glacial cycle (cf. Schäfer et al., 2002; Owen et al., 2005, 2006). The lack of old ages in other study areas of the Himalayan-Tibetan orogen may be the result of poor preservation, particularly in the monsoon-influenced regions where fluvial and mass-movement processes are more dominant. Alternatively, it may be that in other regions, glaciation during the last glacial cycle was extensive enough to have destroyed evidence of early glaciations.

The Karasu glacial stage might be broadly correlated with the Tanggula glacial stage of central Tibet (Owen et al., 2005) and the Indus valley glacial stage in Ladakh (Owen et al., 2006). As Schäfer et al. (2002) and Owen et al. (2005) pointed out, the presence of moraines that predate the last glacial cycle in western Tibet provides strong evidence that an extensive ice sheet, as proposed by Kuhle (e.g., 1985, 1988, 1991, and 1995), could not have existed on the Tibetan Plateau during the last glacial cycle. Had such an ice sheet developed, the glacial and associated landforms from earlier glaciations would have been eroded away. Our data for the Karasu glacial stage moraines confirms the view that an extensive ice sheet did not exist on the Tibetan Plateau during the last glacial cycle. Of course it could be argued that an extremely cold-based ice sheet could have advanced over the landscape doing little erosion to preexisting moraines. However, the relatively well-formed moraines throughout the region do not support this view. Furthermore, there are no landforms, such as meltwater channels, eskers, and kames, in the region that would suggest an extensive Tibetan Plateau ice sheet.

The Subaxh glacial stage probably represents one or more glacial advances during the penultimate glacial cycle and/or the last glacial cycle. These glacier advances resulted in the formation of hummocky moraines developed by piedmont

glaciers. This style of glaciation contrasts with the very extensive ice cap that existed during the Karasu glacial stage and the limited valley glaciers during the Olimde glacial stage. The wide scatter of ages, however, does not allow us to assign each moraine to a specific marine oxygen-isotope stage. Nevertheless, data from the Ting valley (H in Figs. 1–3) suggest that at least one glacial advance was broadly coincident with the global LGM.

Our chronology for the Olimde glacial stage is well defined in comparison to most other TCN surface-exposure dating studies, and is the best numerically defined Holocene glacial succession in the Himalayan-Tibetan orogen. Several of the dated Olimde glacial stage glacial advances that are present within the region are recognized in at least two separate glacier valley systems on the Muztag Ata and Kongur Shan massifs (Figs. 2, 5, and 6). These include moraines: m_{8A} and m_{6C}; m_{7A}, m_{7H}, and m_{3I}; m_{5H} and m_{6H}; m_{5A}, m_{6A}, and m_{4H}; m_{3F} and $m_{3F'}$; and m_{4A}, m_{3C}, and m_{4C}. This provides us with confidence that the moraines and their associated ages represent significant climatically driven events. However, the extent of glaciation for each advance varies significantly within each massif and between the two massifs. This is likely due to differences in hypsometry, aspect, and supply of snow and ice to individual catchments. This makes correlations based on ELA depressions difficult. These problems are discussed in detail in Benn and Lehmkuhl (2000), Owen and Benn (2005), and Seong et al. (2008). Furthermore, several studies have suggested that hypsometry can strongly influence the extent of glaciation, resulting in what may appear to be asynchronous glaciations within a mountain range (Furbish and Andrews, 1984; Kerr, 1993).

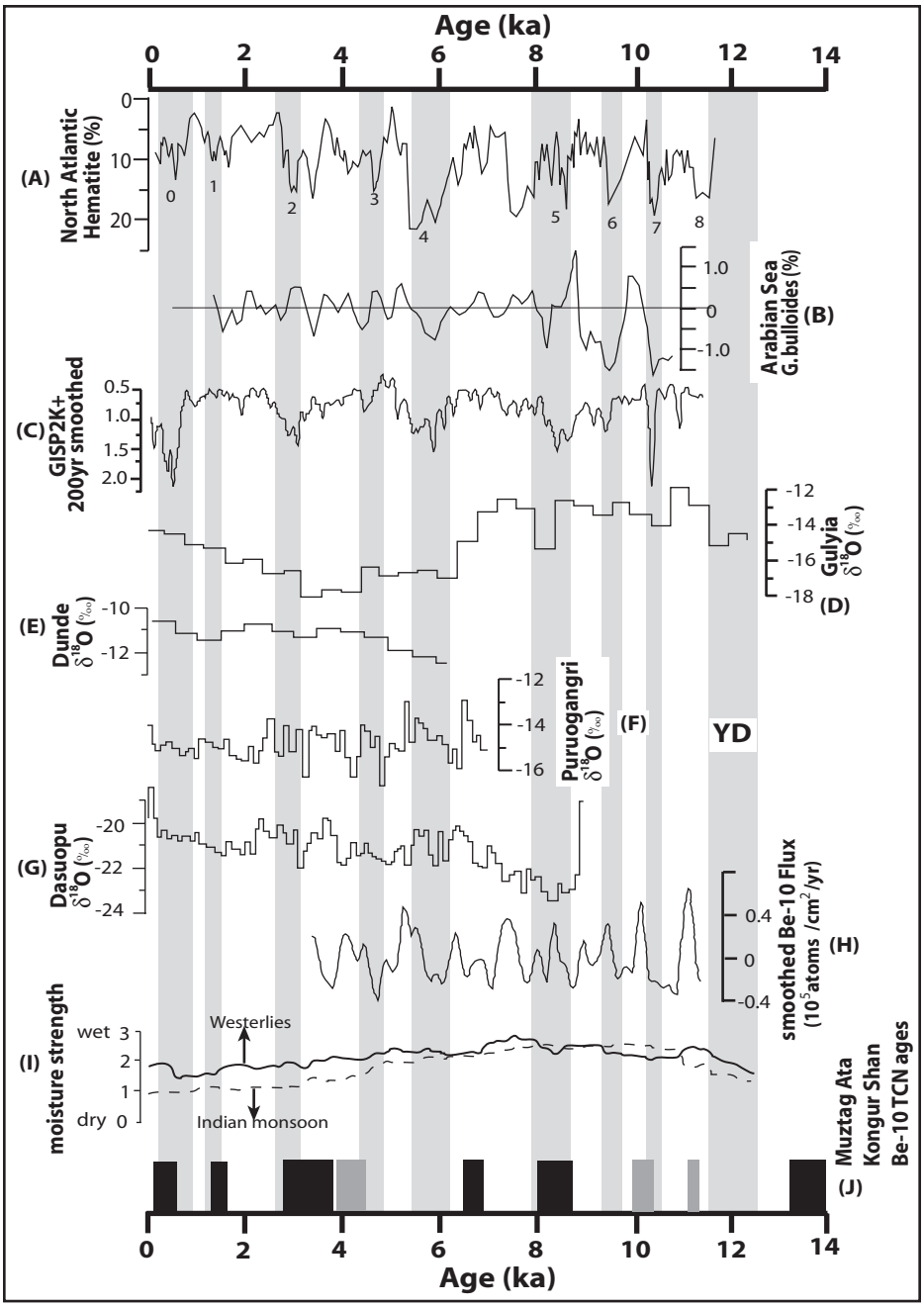

Figure 6. Multiple paleoclimate proxy records of Northern Hemisphere and the Tibetan Plateau during the Holocene. Light-gray bands indicate rapid climate changes after Mayewski et al. (2004). (A) Hematite percentage change in core MC52-VM29–191 from the North Atlantic, and events labeled (1 through 8) in Bond et al. (2001). (B) Percentage change in *Globigenina bulloides* in Bore Hole 723-A from the Arabian Sea (after Gupta et al., 2003). (C) Gaussian smoothed (200 yr) Greenland Ice Sheet Project 2 (GISP2) potassium (K+: ppb) ion proxy for the Siberian high-pressure system (after Meeker and Mayewski, 2002). (D–G) $\delta^{18}O$ record from Guliya, Dundee, Dasuopu, and Purogangri ice core, respectively (after Thompson et al., 1989, 1997, 2005; Thompson, 2000). (H) ^{10}Be production in the GISP2 (Finkel and Nishiizumi, 1997). (I) Effective moisture variability reconstructed from the paleoclimate proxies records of the Tibetan Plateau during the Holocene (Herzschuh, 2006). Solid and dotted curves refer to the westerlies and Indian monsoon, respectively. (J) Holocene glacial events of Muztag Ata–Kongur Shan. The boxes show glacial events centered on 13.7 ka, 11.2 ka, 10.2 ka, 8.4 ka, 6.7 ka, 4.2 ka, 3.3 ka, 1.4 ka, and Little Ice age. The black boxes indicate moraine ages that are present in two or more valleys, while the gray boxes indicate moraine ages that have only been dated in one valley. The center of box marks the mean age of the event and the width of the box for error range. The Younger Dryas Stade is shown as YD. All the ages of proxy records for RCC referenced are corrected calendar ages, whereas cosmogenic ages (J) were calculated from time-constant scaling of geomagnetic intensity change (Lal, 1991; Stone, 2000).

The uncertainties associated with the dating resolution for each of the glacial advances and the scatter of TCN surface-exposure ages do not allow us to precisely assign each glacial advance to a specific global climatic event. Given the quasiperiodicity of the glacial oscillations, however, we suggest these glacial advances correlate with the rapid climate changes that occurred around the Atlantic Ocean from the Late Glacial to the Little Ice Age (LIA) (Bond et al., 1997, 2001; Fig. 6A). Such rapid climate fluctuations are recognized in ice cores from the Greenland ice sheet and in deep-sea sediment cores from the North Atlantic, where a quasiperiodicity of ~1470 yr is apparent throughout the Late Glacial and the Holocene (Bond et al., 1997, 2001; Fig. 6A). This pattern supports the proposed pattern of the Holocene glacial oscillations highlighted by Denton and Karlén (1973). However, we are cautious in making correlations with rapid climate changes when moraines of specific ages are only present in one valley. These include: m_{5H}, m_{6H}, m_{6C}, m_{5C}, m_{3H}, and m_{3A}. Since the TCN surface-exposure ages on these moraines are only for one valley, any correlations with climatostratigraphic events must be considered tentative.

Although there is no unequivocal consensus on the cause of rapid climate oscillations since the global LGM, Mayewski et al. (2004) suggest that for at least the Holocene, changes in insolation related both to Earth's orbital variations and solar variability likely plays a central role in the global scale changes in climate. This quasiperiodicity also correlates reasonably well with fluctuations in the Indian summer monsoon (Gupta et al., 2003; Fig. 6B). Furthermore, these events are well documented in global (Alley et al., 1997; Finkel and Nishiizumi, 1997; Figs. 6C and 6H) as well as in local ice cores (Thompson et al., 1989, 1997, 2005; Thompson, 2000; Figs. 6D to 6G). On the basis of an extensive analysis of multiple proxy data, Herzschuh (2006) showed that the Tibetan Plateau since the global LGM has become increasingly influenced by the midlatitude westerlies, with the exception of the early Holocene when the Indian monsoon dominated (Fig. 6I). Even during the Indian-monsoonal maximum when the strong air uplift caused intensified precipitation and air divergence in the upper troposphere over the Tibetan Plateau, the plateau areas adjacent to our study region experienced an intensified descent of air masses, which consequently decreased the influence of the Indian summer monsoon (Herzschuh, 2006).

The glacier oscillations in this region for the past 18,000 yr were very restricted in extent, within a few kilometers of the contemporary glaciers. This restricted glaciation contrasts sharply with the more extensive glaciations of the monsoon-dominated Himalaya to the south and southeast (Owen et al., 2005). This suggests that the Muztag Ata and Kongur Shan massifs were not significantly influenced by the monsoon but were dominated by the midlatitude westerlies, which brought moisture from the Mediterranean, Black Sea, Caspian Sea, and Aral Sea.

The glacial advance at ca. 17.1 ka might correlate with Heinrich event 1. The following event, at ca. 13.7 ka, is possibly coincident with the Younger Dryas Stade. The two following glaciations (11.2 ka and 10.2 ka) may be synchronous with the Holocene Bond events 7 and 6 that are apparent in North Atlantic deep-sea records (Fig. 6A). Although we argue that the 13.7 ka age moraines formed during the Younger Dryas Stade, this assignment is tentative and is our best estimate based on a combination of TCN chronology and glacial geomorphology. The glacial advance at ca. 8.5 ka may be coincident with a sharp drop in temperature that is likely global in extent (Mayewski et al., 2004; Alley and Ágústsdóttir, 2005; Rohling and Pälike, 2005) and that was probably initiated from catastrophic cold meltwater input into the North Atlantic at 8.47 ka (Barber et al., 1999). The lower temperature at this time, and the likely increased frequencies and magnitude of storm-track development in the region, may have increased the moisture supply to the region (An and Porter, 1997; Alley and Ágústsdóttir, 2005), which in turn likely resulted in positive glacier mass balances allowing glaciers to advance. This combination of relatively high winter accumulation and lower temperature drove the most extensive advance during the Holocene.

The glacial advances between 6.7 ka to a few hundred years ago are also noteworthy. Lake records from the Thar Desert in west India, for example, show that the lake level rose and reached their maximum ca. 7.2–5.5 ka (Enzel et al., 1999). They suggest that winter precipitation, likely provided from the westerlies, accounts for most of the increased total precipitation. This finding is well supported by the decrease in the Indian monsoon (Gupta et al., 2003) and temperature drop in northern Tibet (Thompson et al., 1997). There is no evidence for massive freshwater input into the North Atlantic or for significant Northern Hemisphere ice growth or decay since the ca. 8.5 ka event. Solar variability is a more plausible forcing mechanism for the rapid climate changes that occurred during the middle and late Holocene. In particular, the events at ca. 6.7 ka, ca. 3.3 ka, and the LIA that roughly coincide with maxima in the $\Delta^{14}C$ and $\Delta^{10}Be$ suggest a decline in solar output at these times (Fig. 6H). Although it is difficult to attribute the short durable event at 4.2 ka to a specific forcing mechanism, it is marked by a maximum in ^{10}Be production. This relationship is also supported by southward migration of the Intertropical Convergence Zone (ITCZ), which would be consistent with the increase in strength of the westerlies over the North Atlantic (Hodell et al., 2001). The strengthened westerlies would have increased the winter snowfall as a westerly low-pressure system linked to the North Atlantic pushed farther east along the Himalaya than at present.

During the LIA, total snow accumulation at Dasuopu ice sheet in southern Tibet was 30% higher than the summer amounts in northern India (Thompson, 2000). This was possibly the result of the increased winter snowfall as the westerly low-pressure system linked to the North Atlantic pushed farther east along the Himalaya than it does today. The resultant increased albedo due to increased snowfall and the colder temperatures allowed excess snow and ice to persist late into each year, which may have weakened the subsequent Indian summer monsoon.

The data presented here (Fig. 5A) and the compilation of previous studies that are summarized in Owen et al. (2005) suggest that glacial advances regionally can be broadly, on Milankovich time scales, correlated throughout the Himalaya and Tibet. As in adjacent regions of the Pamir (Zech et al., 2005b) and Ladakh (Owen et al., 2006), which are also dominated by midlatitude westerlies, this region shows a reduction in the extent of glaciation over time. In Pamir, the most extensive glaciation occurred during early last glacial cycle (MIS 4), but in Ladakh it occurred before 400 ka. At the global LGM, the glaciers of both regions had limited advances, restricted to the tributary valleys.

The differences in the extent and timing of glaciation between regions at the western end of the Himalayan-Tibetan orogen imply that even within similar climatic settings, glacial extent and the timing might be affected to different degrees by the topography and variations in regional climate. In the wettest regions, for example, in the Greater Himalaya of northern India, the oldest and most extensive glacial deposits are younger than those in Transhimalaya of northern India, which is one of the driest regions (Owen et al., 2005). This suggests that evidence from old glaciations in wet regions was destroyed by weathering, erosion, and mass movements because of the higher precipitation and increased geomorphic action. In contrast, the drier regions have the oldest and most extensive moraines. The Muztag Ata–Kongur Shan region was dry enough to preserve the oldest and most extensive glacial deposits and landforms that formed prior to the penultimate glacial cycle.

Since the global LGM there has been a decrease in intensity of a Siberian high-pressure system, with the region becoming more exposed to the penetration of westerly moisture mass linked to northern Atlantic climate deteriorations by way of midlatitude westerlies (An and Porter, 1997). Therefore, our new data (Fig. 5) likely support our hypothesis for the importance of midlatitude westerlies in forcing glaciation in semiarid western Tibet.

Our data show that glaciation in the Muztag Ata and Kongur Shan massifs has decreased in extent through time—from ice caps to piedmont glaciers to valley glaciers. This likely represents a significant reduction of the moisture flux to the region over the last few glacial cycles, which is needed to maintain positive glacier mass balances. This possibly reflects a change in regional climatic forcing that might be the result of the progressive surface uplift of the Himalayan ranges on the south and the Pamir to the west, which progressively uplifted and restricted the supply of moisture by the monsoon and westerlies to the region. Owen et al. (2006) recognized a similar change in the extent of glaciation over at least the past 400,000 yr in Ladakh (northern India), which they suggested might be the result of tectonic controls (the progressive uplift of the Himalaya to the south and/or Karakoram Mountains to the west). However, Owen et al. (2006) also recognized that this pattern might reflect a global trend of progressively less extensive mountain glaciation throughout at least the past 400,000 yr. They highlighted that in other mountain regions of the world, such as Tasmania, the Sierra Nevada, Alaska, Peruvian Andes, Patagonia, and the Chilean Lake District, glaciation has also become progressively less extensive over time (Denton et al., 1999; Barrows et al., 2002; Smith et al., 2002; Kaufman et al., 2004; Singer et al., 2004). This suggests that the Northern Hemisphere ice sheets possibly grow at the expense of mountain glaciers over the last several glacial cycles (>400,000 yr).

Alternatively, the change in style of glaciation might represent progressive glacial incision, such that with increased deepening of valleys by glacial erosion the glaciers become progressively more confined to deep valleys. However, this does not explain the reduction in ice volumes. Nevertheless, it is particularly noteworthy that Muztag Ata and Kongur Shan have experienced a seven- to eight-fold accelerated exhumation since 2 million years ago (Arnaud et al., 1993). This rapid exhumation might be broadly equated to the growth of the two massifs, initiating glaciation as ice caps when the massifs became sufficiently high enough to enhance orographic precipitation by the westerlies. During times of deglaciation, meltwater streams would have progressively incised the massif allowing subsequent glacial advances to exploit and deepen the valleys and hence leading to a progression from ice-cap glaciation to valley glaciation.

In essence, our study forms the foundation for future studies on high-mountain glaciers in the semiarid northwestern Tibet and highlights the potential of examining Holocene glacial successions for paleoclimate studies.

CONCLUSIONS

Our new ^{10}Be TCN chronology defines the timing of glaciation for three glacial stages (the Karasu, Subaxh, and Olimde) in the Muztag Ata and Kongur Shan massifs in semiarid westernmost Tibet. The glaciers in this region likely advanced prior to the penultimate glacial cycle (the Karasu glacial stage), the last glacial cycle, and/or during the penultimate glacial cycle (the Subaxh glacial stage) and the Late Glacial and the Holocene (the Olimde glacial stage). Each successive glaciation in the Muztag Ata–Kongur Shan region became progressively less extensive, changing in style from ice caps to piedmont glaciers to restricted valley glaciers. This change in glacial style might be the consequence of tectonic influences on climate and/or topography, or a reflection of a global pattern of glacial change where mountain glaciation has become progressively less extensive in favor of the Northern Hemisphere ice sheet growth.

During Olimde glacial stage (Late Glacial through Holocene), the glaciers of the region advanced at ca. 17.1 ± 0.3 ka, 13.7 ± 0.5 ka, 11.2 ± 0.1 ka, 10.2 ± 0.3 ka, 8.4 ± 0.4 ka, 6.7 ± 0.2 ka, 4.2 ± 0.3 ka, 3.3 ± 0.6 ka, 1.4 ± 0.1 ka, and a few hundred years ago (likely the LIA). This provides the first glacial geologic evidence in the Himalayan-Tibetan orogen that glaciers oscillated in response to quasiperiodicity climate fluctuations on millennial time scales throughout the Late Glacial and Holocene. Furthermore, these data provide the most detailed Late Glacial and Holocene glacial chronology, defined by TCN surface-exposure dating, for any part of the Himalayan-Tibetan orogen. Care must be taken when correlating these moraine ages with climate events, especially when ages are particularly obtained from only one valley. However, when similar ages are obtained from moraines in two or more valleys, we can more confidently assign a glacial advance to a climate event. This is the case for the 13.7 ka, 8.4 ka, 6.7 ka, 1.4 ka, and the LIA glacial advances. These glacier oscillations might be synchronous with ice-rafting events and autocyclicity in the North Atlantic during the Late Glacial and Holocene. This suggests that the record of glacial advances in western Tibet supports the view that atmospheric teleconnections between Tibet and the Northern Hemisphere ice sheets and oceans existed throughout the Late Quaternary. This is also consistent with earlier suggestions that changes in the physical oceanography of the North Atlantic Ocean affect the climate downwind, including the strength and path of storm tracks within the midlatitude westerly system that passes over the semiarid western Tibet. These climatic changes likely forced glaciation during the Late Glacial and Holocene in westernmost Tibet.

ACKNOWLEDGMENTS

Sincere thanks are due to Chinese colleagues (Yabing Li, Gongbi Chen, Ming Chen, and Jianyi Dong) for their help in the field. Special thanks to Associate Editors and reviewers, Eric Kirby, John Gosse, David Evans, Jane Staiger, and Fred Phillips, for their extremely useful and constructive reviews. This research forms part of Yeong Bae Seong's doctoral research, which was partially supported by a Meyers Fellowship at the University of Cincinnati. We would also like to thank National Science Foundation of China for their support for the fieldwork component of this project (NSFC grants 40730101 and 40671023). This work was undertaken at the Lawrence Livermore National Laboratory (LLNL) (under U.S. Department of Energy contract W-7405-ENG-48) as part of an Institute of Geophysics and Planetary Physics/Lawrence Livermore National Laboratory (IGPP/LLNL) research grant. Special thanks to Thomas Lowell for his useful and constructive comments on an early version of this paper.

REFERENCES CITED

Aizen, V., and Aizen, E., 1997, Hydrological cycles on the north and south peripheries of mountain-glacial basins of Central Asia: Hydrological Processes, v. 11, p. 451–469, doi: 10.1002/(SICI)1099-1085(199704)11:5<451::AID-HYP448>3.0.CO;2-M.

Alley, R.B., and Ágústsdóttir, A.M., 2005, The 8 ka event: Cause and consequence of a major Holocene abrupt climate change: Quaternary Science Reviews, v. 24, p. 1123–1149, doi: 10.1016/j.quascirev.2004.12.004.

Alley, R.B., Mayewski, P.A., Sowers, T., Stuiver, M., Taylor, K.C., and Clark, P.U., 1997, Holocene climatic instability: A prominent, widespread event 8200 years ago: Geology, v. 25, p. 483–486, doi: 10.1130/0091-7613(1997)025<0483:HCIAPW>2.3.CO;2.

An Zhisheng, and Porter, S.C., 1997, Millennial-scale climatic oscillations during the last interglaciation in central China: Geology, v. 25, p. 603–606, doi: 10.1130/0091-7613(1997)025<0603:MSCODT>2.3.CO;2.

Arnaud, N.O., Brunel, M., Cantagrel, J.M., and Tapponnier, P., 1993, High cooling and denudation rates at Kongur Shan, eastern Pamir (Xinjiang, China) revealed by ^{40}Ar/^{39}Ar alkali feldspar thermochronology: Tectonics, v. 12, p. 1335–1346, doi: 10.1029/93TC00767.

Barber, D.C., Dyke, A., Hillaire-Marcel, C., Jennings, A.E., Andrews, J.T., Kerwin, M.W., Bilodeau, G., McNeely, R., Southon, J., Morehead, M.D., and Gagnon, J.-M., 1999, Forcing of the cold event of 8,200 years ago by catastrophic drainage of Laurentide lakes: Nature, v. 400, p. 344–348, doi: 10.1038/22504.

Barrows, T.T., Stone, J.O., Fifield, L.K., and Cresswell, R.G., 2002, The timing of the Last Glacial Maximum in Australia: Quaternary Science Reviews, v. 21, p. 159–173, doi: 10.1016/S0277-3791(01)00109-3.

Barry, R.G., and Chorley, R.J., 2003, Atmosphere, weather, and climate (8th edition): New York, Routledge, 279 p.

Benn, D.I., and Lehmkuhl, F., 2000, Mass balance and equilibrium-line altitudes of glaciers in high-mountain environments: Quaternary International, v. 65–66, p. 15–30, doi: 10.1016/S1040-6182(99)00034-8.

Benn, D.I., and Owen, L.A., 2002, Himalayan glacial sedimentary environments: A framework for reconstructing and dating former glacial extents in high mountain regions: Quaternary International, v. 97–98, p. 3–26, doi: 10.1016/S1040-6182(02)00048-4.

Benson, L., Madole, R., Phillips, W., Landis, G., Thomas, T., and Kubik, P., 2004, The probable importance of snow and sediment shielding on cosmogenic ages of north-central Colorado Pinedale and pre-Pinedale moraines: Quaternary Science Reviews, v. 23, no. 2, p. 193–206, doi: 10.1016/j.quascirev.2003.07.002.

Bond, G., Showers, W., Cheseby, M., Lotti, R., Almasi, P., deMenocal, P., Priore, P., Cullen, H., Hajdas, I., and Bonani, G., 1997, A pervasive millennial-scale cycle in North Atlantic Holocene and glacial climates: Science, v. 278, p. 1257–1266, doi: 10.1126/science.278.5341.1257.

Bond, G., Kromer, B., Beer, J., Muscheler, R., Evans, M., Showers, W., Hoffmann, S., Lotti-Bond, R., Hajdas, I., and Bonani, G., 2001, Persistent solar influence on North Atlantic climate during the Holocene: Science, v. 294, p. 2130–2136, doi: 10.1126/science.1065680.

Brunel, M., Arnaud, N., Tapponnier, P., Pan, Y., and Wang, Y., 1994, Kongur Shan normal fault: Type example of mountain building assisted by extension (Karakoram fault, eastern Pamir): Geology, v. 22, p. 707–710, doi: 10.1130/0091-7613(1994)022<0707:KSNFTE>2.3.CO;2.

Denton, G.H., and Karlén, W., 1973, Holocene climatic variations: Their pattern and possible cause: Quaternary Research, v. 3, p. 155–205, doi: 10.1016/0033-5894(73)90040-9.

Denton, G.H., Heusser, C.J., Lowell, T.V., Moreno, P.I., Anderson, B.G., Heusser, L.E., Schlüchter, C., and Marchant, D.R., 1999, Interhemispheric linkage of paleoclimate during the last glaciation: Geografiska Annaler, v. 81A, p. 107–154, doi: 10.1111/j.0435-3676.1999.00055.x.

Derbyshire, E., 1981, Glacier regime and glacial sediment facies: A hypothetical framework for the Qinghai-Xizang Plateau, *in* Geological and ecological studies of Qinghai-Xizang Plateau: Beijing, Proceedings of Symposium on Qinghai-Xizang (Tibet) Plateau, Science Press, v. 2, p. 1649–1656.

Derbyshire, E., 1983, The Lushan dilemma: Pleistocene glaciation south of the Chang Jiang (Yangtze River): Zeitschrift für Geomorphologie, v. 27, p. 445–471.

Enzel, Y., Ely, L.L., Mishra, S., Ramesh, R., Amit, R., Lazar, B., Rajaguru, S.N., Baker, B.R., and Sandler, A., 1999, High-resolution Holocene environmental changes in the Thar Desert, northwestern India: Science, v. 284, p. 125–128, doi: 10.1126/science.284.5411.125.

Finkel, R.C., and Nishiizumi, K., 1997, Beryllium-10 concentrations in the Greenland Ice Sheet Project 2 ice core from 3–40 ka: Journal of Geophysical Research, v. 102, p. 26,699–26,706, doi: 10.1029/97JC01282.

Finkel, R.C., Owen, L.A., Barnard, P.L., and Caffee, M.W., 2003, Beryllium-10 dating of Mount Everest moraines indicates a strong monsoonal influence and glacial synchroneity throughout the Himalaya: Geology, v. 31, p. 561–564.

Fort, M., and Peulvast, J., 1995, Catastrophic mass-movements and morphogenesis in the peri-Tibetan Ranges: Examples for West Kunlun, East Pamir and Ladakh, *in* Slaymaker, O., ed., Steepland Geomorphology: Chichester, UK, Wiley, p. 171–198.

Furbish, D.J., and Andrews, J.T., 1984, The use of hypsometry to indicate long-term stability and response of valley glaciers to changes in mass transfer: Journal of Glaciology, v. 105, p. 199–211.

Gillespie, A., and Molnar, P., 1995, Asynchronous maximum advances of mountain and continental glaciers: Reviews of Geophysics, v. 33, p. 311–364, doi: 10.1029/95RG00995.

Gosse, J.C., and Phillips, F.M., 2001, Terrestrial in situ cosmogenic nuclides: Theory and application: Quaternary Science Reviews, v. 20, p. 1475–1560, doi: 10.1016/S0277-3791(00)00171-2.

Gupta, A.K., Anderson, D.M., and Overpeck, J.T., 2003, Abrupt changes in the Asian southwest monsoon during the Holocene and their links to the North Atlantic Ocean: Science, v. 421, p. 354–357.

Herzschuh, U., 2006, Paleo-moisture evolution in monsoonal Central Asia during the last 50,000 years: Quaternary Science Reviews, v. 25, p. 163–178, doi: 10.1016/j.quascirev.2005.02.006.

Hewitt, K., 1999, Quaternary moraines vs catastrophic avalanches in the Karakoram Himalaya, northern Pakistan: Quaternary Research, v. 51, p. 220–237, doi: 10.1006/qres.1999.2033.

Hodell, D.A., Brenner, M., Curtis, J.H., and Guilderson, T., 2001, Solar forcing of drought frequency in the Maya Lowlands: Science, v. 292, p. 1367–1370, doi: 10.1126/science.1057759.

Hughes, P.D., Gibbard, P.L., and Woodward, J.C., 2005, Quaternary glacial records in mountain regions: A formal stratigraphical approach: Episodes, v. 28, no. 2, p. 85–92.

Kaufman, D.S., Porter, S.C., and Gillespie, A.R., 2004, Quaternary alpine glaciations in Alaska, the Pacific Northwest, Sierra Nevada, and Hawaii, *in* Gillespie, A.R., Porter, S.C., and Atwater, B.F., eds., The Quaternary Period in the United States: Developments in Quaternary Science, v. 1: Amsterdam, Netherlands, Elsevier p. 77–104.

Kerr, A., 1993, Topography, climate and ice masses: A review: Terra Nova, v. 5, p. 332–342.

Kohl, C. P., and Nishiizumi, K., 1992, Chemical isolation of quartz for measurement of in-situ produced cosmogenic nuclides: Geochimica et Cosmochimica Acta, v. 56, p. 3583–3587.

Kuhle, M., 1985, Glaciation research in the Himalayas: A new ice age theory: Universitas, v. 27, p. 281–294.

Kuhle, M., 1988, Geomorphological findings on the build-up of Pleistocene glaciation in southern Tibet and on the problem of inland ice: Results of the Shisha Pangma and Mt. Everest: Geojournal, v. 17, p. 457–511.

Kuhle, M., 1991, Observations supporting the Pleistocene inland glaciation of High Asia: GeoJournal, v. 25, p. 131–231, doi: 10.1007/BF02682190.

Kuhle, M., 1995, Glacial isostatic uplift of Tibet as a consequence of a former ice sheet: GeoJournal, v. 37, p. 431–449, doi: 10.1007/BF00806933.

Lal, D., 1991, Cosmic ray labeling of erosion surfaces: in situ nuclide production rates and erosion models: Earth and Planetary Science Letters, v. 104, p. 424–439, doi: 10.1016/0012-821X(91)90220-C.

Lal, D., Harris, N.B.W., Sharma, K.K., Gu, Z., Ding, L., Liu, T., Dong, W., Caffee, M.W., and Jull, A.J.T., 2004, Erosion history of the Tibetan Plateau since the last interglacial: constrains from the first studies of cosmogenic ^{10}Be from Tibetan bedrock: Earth and Planetary Science Letters, v. 217, p. 33–42, doi: 10.1016/S0012-821X(03)00600-9.

Mayewski, P.A., Rohling, E.E., Stager, C.J., Karlen, W., Maasch, A., Meeker, L.D., Meyerson, E.A., Gasse, F., Van Kreveld, S., Holmgren, K., Lee-Thorp, J., Rosqvist, G., Rack, F., Staubwasser, M., Schneider, R.R., and Steig, E.J., 2004, Holocene climate variability: Quaternary Research, v. 62, p. 243–255, doi: 10.1016/j.yqres.2004.07.001.

Meeker, L.D., and Mayewski, P.A., 2002, A 1400-year high-resolution record of atmospheric circulation over the North Atlantic and Asia: The Holocene, v. 12, p. 257–266, doi: 10.1191/0959683602hl542ft.

Miehe, G., Winiger, M., Bohner, J., and Yili, Z., 2001, Climatic diagram map of High Asia: Purpose and concepts: Erdkunde, v. 55, p. 94–97, doi: 10.3112/erdkunde.2001.01.06.

Mix, A.C., Bard, E., and Schneider, R., 2001, Environmental processes of the ice age: Land, ocean, glaciers (EPILOG): Quaternary Science Reviews, v. 20, p. 627–657, doi: 10.1016/S0277-3791(00)00145-1.

Molnar, P., and England, P., 1990, Late Cenozoic uplift and global climate change: Chicken or egg?: Nature, v. 346, p. 29–34, doi: 10.1038/346029a0.

Nishiizumi, K., Winterer, E.L., Kohl, C.P., Lal, D., Arnold, J.R., Klein, J., and Middleton, R., 1989, Cosmic ray production rates of ^{10}Be and ^{26}Al in quartz from glacially polished rocks: Journal of Geophysical Research, v. 94, p. 17,907–17,915, doi: 10.1029/JB094iB12p17907.

Nishiizumi, K., Imamura, M., Caffee, M.W., Southon, J.R., Finkel, R.C., and McAninch, J., 2007, Absolute calibration of ^{10}Be AMS Standards: Nuclear Instruments and Methods in Physical Research Section, v. 258, no. 2, p. 403–413, doi: 10.1016/j.nimb.2007.01.297.

Ono, Y., Liu, D., and Zhao, Y., 1997, Paleoenvironment of Tibetan Plateau from glacial fluctuations in the northern foot of the West Kunlun Mountains: The Journal of Geography, v. 106, p. 184–198.

Owen, L.A., 1991, Mass movement deposits in the Karakoram Mountains: Their sedimentary characteristics, recognition and role in Karakoram landform evolution: Zeitschrift für Geomorphologie, v. 35, p. 401–424.

Owen, L.A., and Benn, D.I., 2005, Equilibrium-line altitudes of the Last Glacial Maximum for the Himalaya and Tibet: An assessment and evaluation of results: Quaternary International, v. 138–139, p. 55–78, doi: 10.1016/j.quaint.2005.02.006.

Owen, L.A., Derbyshire, E., and Fort, M., 1998, The Quaternary glacial history of the Himalaya; a review, *in* Owen, L.A., ed., Mountain Glaciation: Quaternary Proceedings, Cambridge, UK: Quaternary Research Association, v. 6, p. 91–120.

Owen, L.A., Gualtieri, L., Finkel, R.C., Caffee, M.W., Benn, D.I., and Sharma, M.C., 2001, Cosmogenic radionuclide dating of glacial landforms in the Lahul Himalaya, northern India: Defining the timing of Late Quaternary glaciation: Journal of Quaternary Science, v. 16, p. 555–563, doi: 10.1002/jqs.621.

Owen, L.A., Finkel, R.C., and Caffee, M.W., 2002a, A note on the extent of glaciation in the Himalaya during the global Last Glacial Maximum: Quaternary Science Reviews, v. 21, p. 147–157, doi: 10.1016/S0277-3791(01)00104-4.

Owen, L.A., Finkel, R.C., Caffee, M.W., and Gualtieri, L., 2002b, Timing of multiple Late Quaternary glaciations in the Hunza Valley, Karakoram Mountains, northern Pakistan: Defined by cosmogenic radionuclide dating of moraines: Geological Society of America Bulletin, v. 114, p. 593–604, doi: 10.1130/0016-7606(2002)114<0593:TOMLQG>2.0.CO;2.

Owen, L.A., Kamp, U., Spencer, J.Q., and Haserodt, K., 2002c, Timing and style of Late Quaternary glaciation in the eastern Hindu Kush, Chitral, northern Pakistan: A review and revision of the glacial chronology based on new optically stimulated luminescence dating: Quaternary International, v. 97–98, p. 41–55, doi: 10.1016/S1040-6182(02)00050-2.

Owen, L.A., Spencer, J.Q., Ma, H., Barnard, P.L., Derbyshire, E., Finkel, R.C., Caffee, M.W., and Zeng, Y.N., 2003a, Timing of Late Quaternary glaciation along the southwestern slopes of the Qilian Shan: Tibet: Boreas, v. 32, p. 281–291, doi: 10.1080/03009480310001632.

Owen, L.A., Finkel, R.C., Ma, H., Spencer, J.Q., Derbyshire, E., Barnard, P.L., and Caffee, M.W., 2003b, Timing and style of Late Quaternary glaciations in NE Tibet: Geological Society of America Bulletin, v. 115, p. 1356–1364, doi: 10.1130/B25314.1.

Owen, L.A., Finkel, R.C., Minnich, R., and Perez, A., 2003c, Extreme southern margin of Late Quaternary glaciation in North America: Timing and controls: Geology, v. 31, p. 729–732, doi: 10.1130/G19561.1.

Owen, L.A., Finkel, R.C., Barnard, P.L., Haizhhou, M., Asahi, K., Caffee, M.W., and Derbyshire, E., 2005, Climatic and topographic controls on the style and timing of Late Quaternary glaciation throughout Tibet and the Himalaya defined by ^{10}Be cosmogenic radionuclide surface exposure dating: Quaternary Science Reviews, v. 24, p. 1391–1411, doi: 10.1016/j.quascirev.2004.10.014.

Owen, L.A., Caffee, M.W., Bovard, K.R., Finkel, R.C., and Sharma, M.C., 2006, Terrestrial cosmogenic nuclide surface exposure dating of the oldest glacial successions in the Himalayan orogen: Ladakh Range, northern India: Geological Society of America Bulletin, v. 118, no. 3–4, p. 383–392, doi: 10.1130/B25750.1.

Phillips, W.M., Sloan, V.F., Shroder, J.F., Jr., Sharma, P., Clarke, M.L., and Rendell, H.M., 2000, Asynchronous glaciation at Nanga Parbat, northwestern Himalaya Mountains, Pakistan: Geology, v. 28, p. 431–434, doi: 10.1130/0091-7613(2000)28<431:AGANPN>2.0.CO;2.

Pigati, J.S., and Lifton, N.A., 2004, Geomagnetic effects on time-integrated cosmogenic nuclide production with emphasis on in situ ^{14}C and ^{10}Be: Earth and Planetary Science Letters, v. 226, p. 193–205, doi: 10.1016/j.epsl.2004.07.031.

Porter, S.C., 1970, Quaternary glacial record in Swat Kohistan, West Pakistan: Geological Society of America Bulletin, v. 81, p. 1421–1446, doi: 10.1130/0016-7606(1970)81[1421:QGRISK]2.0.CO;2.

Prell, W.L., and Kutzbach, J.F., 1992, Sensitivity of the Indian monsoon to forcing parameters and implications for its evolution: Nature, v. 360, p. 647–652, doi: 10.1038/360647a0.

Richards, B.W.M., Owen, L.A., and Rhodes, E.J., 2000a, Timing of Late Quaternary glaciations in the Himalayas of northern Pakistan: Journal of Quaternary Science, v. 15, p. 283–297, doi: 10.1002/(SICI)1099-1417(200003)15:3<283::AID-JQS525>3.0.CO;2-X.

Richards, B.W.M., Benn, D., Owen, L.A., Rhodes, E.J., and Spencer, J.Q., 2000b, Timing of Late Quaternary glaciations south of Mount Everest in the Khumbu Himal, Nepal: Geological Society of America Bulletin, v. 112, p. 1621–1632, doi: 10.1130/0016-7606(2000)112<1621:TOLQGS>2.0.CO;2.

Robinson, A.C., Yin, A., Manning, C.E., Harrison, T.M., Zhang, S.H., and Wang, X.F., 2004, Tectonic evolution of the north eastern Pamir: Constraints from the portion of the Cenozoic Kongur Shan extensional system, western China: Geological Society of America Bulletin, v. 116, no. 7–8, p. 953–973, doi: 10.1130/B25375.1.

Rohling, E.J., and Pälike, H., 2005, Centennial-scale climate cooling with a sudden cold event around 8,200 years ago: Nature, v. 434, p. 975–979, doi: 10.1038/nature03421.

Rose, J., and Menzies, J., 1995, Glacial stratigraphy, *in* Menzies, J., ed., Past glacial environments: Sediments, forms and techniques: Oxford, Butterworth Heinemann, p. 253–284.

Ruddiman, W.F., and Kutzbach, J.E., 1989, Late Cenozoic plateau uplift and climate change: Transactions of the Royal Society of Edinburgh: Earth Sciences, v. 81, p. 301–341.

Schäfer, J.M., Tshudi, S., Zhizhong, Z., Sihao, W., Ivyochs, S., Wieler, R., Baur, H., Kubik, P.W., and Schluchter, C., 2002, The limited influence of glaciation in Tibet on global climate over the past 170,000 yr: Earth and Planetary Science Letters, v. 194, p. 287–297, doi: 10.1016/S0012-821X(01)00573-8.

Schoenbohm, L., Chen, J., Sobel, E., Thiede, R., and Strecker, M., 2005, Glacial erosion, deep exhumation and the development of high topography along the Kongur detachment, Pamir Mountains, Western China*:* Eos (Transactions, American Geophysical Union), v. 86, no. 52, p. T23C-0576.

Seong, Y.B., Owen, L.A., Yi, C., Finkel, R.C., and Schoenbohm, L., 2008, Geomorphology of anomalously high glaciated mountains at the northwestern end of Tibet: Muztag Ata and Kongur Shan: Geomorphology, doi: 10.1016/j.geomorph.2008.04.025 (in press).

Sharma, M.C., and Owen, L.A., 1996, Quaternary glacial history of the Garhwal Himalaya, India: Quaternary Science Reviews, v. 15, p. 335–365, doi: 10.1016/0277-3791(95)00061-5.

Shi, Y., 2002, Characteristics of late Quaternary monsoonal glaciation on the Tibetan Plateau and in East Asia: Quaternary International, v. 97–98, p. 79–91, doi: 10.1016/S1040-6182(02)00053-8.

Shroder, J.F., Owen, L.A., and Derbyshire, E., 1993, Quaternary glaciation of the Karakoram and Nanga Parbat Himalaya, *in* Shroder, J.F., ed., Himalaya to the sea: Geology, geomorphology and the Quaternary: London, Routledge, p. 132–158.

Singer, B.S., Ackert, R.P., and Guillou, H., 2004, $^{40}Ar/^{39}Ar$ and K-Ar chronology of Pleistocene glaciations in Patagonia: Geological Society of America Bulletin, v. 116, p. 434–450, doi: 10.1130/B25177.1.

Skrine, C.P., 1925, The alps of Qungur: The Geographical Journal, v. 66, no. 5, p. 385–407, doi: 10.2307/1782660.

Small, E.E., Anderson, R.S., Repka, J.L., and Finkel, R.C., 1997, Erosion rates of alpine bedrock summit surfaces deduced from in situ Be-10 and Al-26: Earth and Planetary Science Letters, v. 150, p. 413–425, doi: 10.1016/S0012-821X(97)00092-7.

Smith, J.A., Farber, D.L., Seltzer, G.O., Finkel, R.C., and Rodbell, D.T., 2002, Chronology of tropical glaciation from cosmogenic dating: Eos (Transactions, American Geophysical Union), v. 83, no. 47, p. F922.

Staiger, J., Gosse, J., Toracinta, R., Oglesby, B., Fastook, J., and Johnson, J.V., 2007, Atmospheric scaling of cosmogenic nuclide production: Climate effect: Journal of Geophysical Research-Solid Earth: v. 112, B02205, doi: 10.1029/2005JB003811.

Stone, J.O., 2000, Air pressure and cosmogenic isotope production: Journal of Geophysical Research, v. 105, no. B10, p. 23,753–23,759, doi: 10.1029/2000JB900181.

Thackray, G., Owen, L.A., and Yi, C., 2008, eds., Late Quaternary mountain glaciation: Journal of Quaternary Science, v. 23, p. 503–702.

Tapponnier, P., Peltzer, G., Le Dain, A.Y., Armijo, R., and Cobbold, P., 1982, Propagating extrusion tectonics in Asia: New insights from simple experiments with plasticity: Geology, v. 10, p. 611–616, doi: 10.1130/0091-7613(1982)10<611:PETIAN>2.0.CO;2.

Thompson, L.G., 2000, Ice core evidence for climate change in the Tropics: Implications for our future: Quaternary Science Reviews, v. 19, p. 19–35, doi: 10.1016/S0277-3791(99)00052-9.

Thompson, L.G., Mosley-Thompson, E., Davis, M.E., Bolzan, J.F., Dai, J., Yao, T., Gundestrup, N., Wu, X., Klein, L., and Xie, Z., 1989, Holocene–Late Pleistocene climatic ice core records from Qinghai-Tibetan Plateau: Science, v. 246, p. 474–477, doi: 10.1126/science.246.4929.474.

Thompson, L.G., Yao, T., Davis, M.E., Henderson, K.A., Mosley-Thompson, E., Lin, P.-N., Beer, J., Synal, H.A., Cole-Dai, J., and Bolzan, J.F., 1997, Tropical climate instability: The last glacial cycle from a Qinghai-Tibetan ice core: Science, v. 276, p. 1821–1825, doi: 10.1126/science.276.5320.1821.

Thompson, L.G., Davis, M.E., Mosley-Thompson, E., Lin, P.-N., Henderson, K.A., and Mashiotta, T.A., 2005, Tropical ice core records: Evidence for asynchronous glaciation on Milankovitch timescales: Journal of Quaternary Science, v. 20, no. 7–8, p. 723–733, doi: 10.1002/jqs.972.

Tsukamoto, S., Asdahi, K., Watanabe, T., Kondo, R., and Rink, W.J., 2002, Timing of past glaciation in Kanchenjunga Himal, Nepal by optically stimulated luminescence dating of tills: Quaternary International, v. 97–98, p. 57–68, doi: 10.1016/S1040-6182(02)00051-4.

Wake, C.P., Mayewski, P.A., and Han, J., 1994, Modern eolian dust deposition in Central Asia: Tellus, v. 46B, p. 220–233.

Zech, R., Glase, B., Sosin, P., Kubik, P.W., and Zech, W., 2005a, Evidence for long-lasting landform surface instability on hummocky moraines in the Pamir Mountains (Tajikistan) from ^{10}Be surface exposure dating: Earth and Planetary Science Letters, v. 237, p. 453–461, doi: 10.1016/j.epsl.2005.06.031.

Zech, R., Abramowki, U., Glaser, B., Sosin, P., Kubik, P.W., and Zech, W., 2005b, Late Quaternary glacial and climate history of the Pamir Mountains derived from cosmogenic ^{10}Be exposure ages: Quaternary Research, v. 64, p. 212–220, doi: 10.1016/j.yqres.2005.06.002.

Zehfuss, P.H., Bierman, P.R., Gillespie, A.R., Burke, R.A., and Caffee, M.C., 2001, Slip rates on the Fish Springs fault, Owens Valley, California, deduced from cosmogenic ^{10}Be and ^{26}Al and soil development on fan surfaces: Geological Society of America Bulletin, v. 113, p. 241–255, doi: 10.1130/0016-7606(2001)113<0241:SROTFS>2.0.CO;2.

Manuscript Received 9 October 2007
Revised Manuscript Received 2 July 2008
Manuscript Accepted 24 July 2008

Printed in the USA